ARTICLE IN PRESS

Icarus xxx (xxxx) xxx

Contents lists available at ScienceDirect

Icarus

journal homepage: www.elsevier.com/locate/icarus

A comparison of CO_2 seasonal activity in Mars' northern and southern hemispheres

C.J. Hansen [a,*], S. Byrne [b], W.M. Calvin [c], S. Diniega [d], C.M. Dundas [e], P.O. Hayne [f], A.S. McEwen [g], L.E. McKeown [d], S. Piqueux [d], G. Portyankina [h], M.E. Schwamb [i], T.N. Titus [e], J.M. Widmer [j]

[a] Planetary Science Institute, Tucson, AZ, United States of America
[b] Lunar and Planetary Laboratory, University of Arizona, AZ, United States of America
[c] Department of Geological Sciences, University of Nevada, Reno, NV, United States of America
[d] Jet Propulsion Laboratory, California Institute of Technology, CA, United States of America
[e] U.S. Geological Survey, Astrogeology Science Center, 2255 N. Gemini Dr., Flagstaff, AZ, United States of America
[f] Laboratory for Atmospheric and Space Physics, University of Colorado, Boulder, United States of America
[g] Lunar and Planetary Lab, University of Arizona, Tucson, AZ, United States of America
[h] German Aerospace Center, DLR, Rutherfordstrasse 2, 12489 Berlin, Germany
[i] Astrophysics Research Centre, School of Mathematics and Physics, Queen's University Belfast, Belfast BT7 1NN, UK
[j] University of California, Los Angeles, CA, United States of America

ARTICLE INFO

Keywords:
Mars' seasons
Mars' CO2 ice
Mars climate

ABSTRACT

Carbon dioxide is Mars' most active volatile. The seasonal and diurnal processes of when and where it condenses and sublimates are determined by energy balance between the atmosphere and surface ice in Mars' vapor pressure equilibrium climate. Mars' current obliquity ensures that the polar caps are stable locations for seasonal condensation. The eccentricity of Mars' orbit is the major driver of differences in seasonal behavior of CO_2 between the northern vs southern hemisphere. In particular, the current positions of perihelion and aphelion, in addition to the large elevation difference between the poles, dominate the ways seasonal processes transpire in the two hemispheres. We summarize and discuss the unprecedented observations of these processes that have been collected by the Mars Reconnaissance Orbiter over the last 8.5 Mars Years. The longer southern fall and winter allows more time for CO_2 ice to accumulate and densify in the southern hemisphere. Northern winter coincides with the perihelion dust storm season, thus the north polar seasonal ice deposits are expected to contain a greater concentration of dust in relation to CO_2 and H_2O ices. With less time for densification and more contaminants the northern seasonal layer of CO_2 ice is likely weaker than the southern layer.

1. Introduction

The waxing and waning of Mars' seasonal polar caps has been observed from earth for multiple centuries (Herschel, 1784; James et al., 1992). Prior to spacecraft observations the dominant composition of the seasonal ice was controversial. In the late eighteenth century, Herschel (1784) was the first to observe the dynamic nature of the polar caps and believed that the polar caps were composed of H_2O ice; this was the popular belief for almost two centuries. We now know that the seasonal polar caps are predominantly composed of CO_2 ice with minor but variable amounts of water ice and dust (Neugebauer et al., 1971; Calvin and Martin, 1994; Kieffer and Titus, 2001; Langevin et al., 2007a). Furthermore, Mars' seasonal processes are dominated by the sublimation and condensation of CO_2 in its vapor pressure equilibrium-controlled climate (e.g., Leighton and Murray, 1966; Mischna et al., 2003), with ~25% of the atmosphere being annually cycled to the surface as CO_2 ice and snow (Tillman et al., 1993; Kelly et al., 2006). Surface activity associated with sublimation of the seasonal ice was first imaged in detail by the Mars Observer Camera on the Mars Global Surveyor (Malin and Edgett, 2001).

Understanding the seasonal polar cap has been an ongoing topic of interest to better constrain the polar energy budget and interannual

* Corresponding author.
E-mail address: cjhansen@psi.edu (C.J. Hansen).

https://doi.org/10.1016/j.icarus.2023.115801
Received 17 May 2023; Received in revised form 30 August 2023; Accepted 14 September 2023
Available online 19 September 2023

variability. The seasonal cap has been investigated in both hemispheres with visible (Calvin et al., 2015, 2017; Acharya et al., 2023), thermal (Piqueux et al., 2015a; Bapst et al., 2015), laser altimetric (Smith et al., 2001b; Aharonson et al., 2004), and spectral (Brown et al., 2010, 2012; Schmidt et al., 2010) observations. Results from these studies in the form of longitudinally averaged maps of retreat rates of the seasonal ice are largely consistent across data types with minor variations attributed to differences in resolution or seasonal cap edge definitions (Calvin et al., 2017). However, significant interannual variability is observed, particularly near the margins of the residual ice domes, which retain high albedo deposits in some locations in some years but not in others (e.g. Calvin et al., 2015, 2017; Thomas et al., 2020). Planet-encircling dust events have been noted to influence short term retreat rates (e.g. Piqueux et al., 2015a; Acharya et al., 2023).

In-situ atmospheric pressure follows an annual repeatable cycle, as noted in both Viking (Tillman et al., 1993) and Curiosity (Ordonez-Etxeberria et al., 2019) datasets. The minimum of this cycle is reached during southern winter. Due to orbital eccentricity, the timing of aphelion, and higher elevation, the southern winter is both longer in duration and colder than the northern winter. This results in more extensive coverage by seasonal ice in the south and the deepest minimum of the pressure curve in this season.

One of the most important findings of the Mars Global Surveyor (MGS) and Mars Reconnaissance Orbiter (MRO) missions is that geologic processes that shape the surface are active in Mars' current climate, not confined to the environment and events of billions of years ago. In addition to the weather, erosional and depositional processes on the surface are driven by the CO_2 cycle and winds (summarized in Diniega et al., 2021). Sublimation of the seasonal CO_2 cap that condenses on the winter pole is responsible for carving enigmatic spider-like channels known as araneiform terrain (Kieffer et al., 2000, 2006; Kieffer, 2007; Piqueux et al., 2003; Piqueux and Christensen, 2008), dendritic troughs (Portyankina et al., 2017) and furrows on dunes (Hansen et al., 2013). Additionally, extensive monitoring by MRO has demonstrated that gully activity correlates with the presence and springtime sublimation of CO_2 frost and is likely contributing to ongoing gully formation (Diniega et al., 2010; Dundas et al., 2012, 2015, 2019; Vincendon, 2015).

In this paper we explore the differences in seasonal processes in the northern vs. southern hemispheres. If Mars were a sphere in a circular orbit the seasonal polar cap boundaries and seasonal processes would be symmetrical. It is not, however, and seasonal activity is much more complex. Mars' orbit is elliptical, thus differences in insolation as the Mars year unfolds drive north-south differences. The elevation differences between the northern and southern polar caps are substantive. Geological differences are important when making this comparison. Seasonal processes have been described for individual hemispheres, but not thoroughly compared and contrasted. We focus primarily on the behavior of CO_2, even though water is an important, albeit minor, constituent in the north polar cap. We rely extensively on datasets from MRO, which now cover almost a full martian decade. One of the most important capabilities of MRO is routine off-nadir pointing, enabling repeat coverage of individual sites to track surface changes throughout a season and across multiple Mars years.

1.1. Densification of CO_2 ice

Throughout this paper we use the generic term densification to summarize the processes that lead to a translucent slab of CO_2 ice. Seasonal CO_2 may accumulate on the surface through direct condensation or snowfall. In their original model, Kieffer et al. (2006); Kieffer, 2007 envisioned deposition of solid ice and used the term annealing to describe the process of sealing cracks and pores. Snowfall may also be converted from a granular deposit to a connected, albeit porous, slab by sintering. Models of pressureless sintering of CO_2 snowfall on Mars indicate this process is rapid enough to be relevant to martian seasonal deposits (Eluszkiewicz and Moncet, 2003; Eluszkiewicz et al., 2005; Cornwall and Titus, 2009, 2010). After sintering, cracks and pores in the ice can also be progressively sealed in an annealing process similar to what Kieffer envisioned in directly deposited ice (Mc Keown et al., 2023). Both processes may be operating on Mars today at different times in different locations (or different vertical levels at the same location). Indeed, the difference in how both terms have been used may be largely semantic. Eluszkiewicz et al. (2005) suggested the instantaneous formation of a non-porous slab can be rationalized as the rapid sintering of sufficiently small snow particles. In our discussion of the seasonal effects of translucent ice we remain agnostic on the microphysical processes at work but highlight it as an area worthy of continued study.

1.2. Mars Reconnaissance Orbiter

MRO was launched in 2005 carrying six scientific instruments (Zurek and Smrekar, 2007): the High Resolution Imaging Science Experiment (HiRISE; McEwen et al., 2007), the Compact Reconnaissance Imaging Spectrometer for Mars (CRISM; Murchie et al., 2007), the Shallow Radar (SHARAD; Seu et al., 2007), the Context Camera (CTX; Malin et al., 2007), the Mars Colour Imager (MARCI; Malin et al., 2001), and the Mars Climate Sounder (MCS; McCleese et al., 2007). MRO reached the $\sim$255 × 320 km Mars mapping orbit in November of 2006, at $L_s = 13\hat{2}°$ of Mars Year (MY) 28 (see Piqueux et al., 2015b for an explanation of Mars Years). The orbit is nearly but not exactly polar, as needed to maintain a sun-synchronous orbit near 3 PM local time at the dayside equator. With routine cross-track pointing up to 30°, all of Mars can be observed by HiRISE, CRISM, and CTX (as well as MARCI).

MRO has been active in its mapping orbit from northern summer in MY28 to early MY37 (as of April 2023), over 8.5 Mars Years. There have been global dust storms in MY28 and MY34 (Kass et al., 2020), as well as large regional dust storms in other years. A set of papers in this issue describe operations and science results from MRO over this time period (McEwen et al., 2023; Landis, 2023). Multi-year datasets are enabling investigations of dynamic processes that go beyond snapshots in time. While combining datasets that provide different points of view to the same phenomena are important for short-term studies, multi-year data are crucial for understanding relationships between short- and long-term and transient phenomena. These correlation studies with the use of extended datasets are instrumental for understanding the physics behind dynamic processes that repeat yearly for decades.

2. Hemispheric geologic settings

We begin with a review of the geological settings, comparing north and south extended polar regions. All of these regions have been the topic of multiple papers and books, so we focus just on the attributes that are likely to affect seasonal processes. Mars has a major hemispheric dichotomy in elevation (Smith et al., 2001a): the northern elevation poleward of 55° N is generally 4–5 km below global average, while the southern elevation poleward of 55° S is typically 1–4 km above global average (Fig. 1). The south polar region is largely old rugged cratered highlands while the north polar surface layer is younger and smoother at the km scale as older terrain is mostly covered by sediments and lava plains units (Tanaka et al., 2014). In addition to these hemispheric differences, the terrain types, materials, depth to ice, thermal inertia of the substrate, and topography all vary on local and regional scales.

2.1. Permanent polar caps and layered deposits

Each pole hosts a thick stack of layered deposits and a thin residual polar ice cap that remains in the summer after the seasonal ice is gone. The top of the north polar residual cap (NPRC) is water ice. The highest albedo layer of the south polar residual cap (SPRC) is CO_2; however, water ice is exposed in intermediate albedo units at the periphery of the CO_2 (Doute et al., 2007; Piqueux et al., 2008; Cartwright et al., 2022;

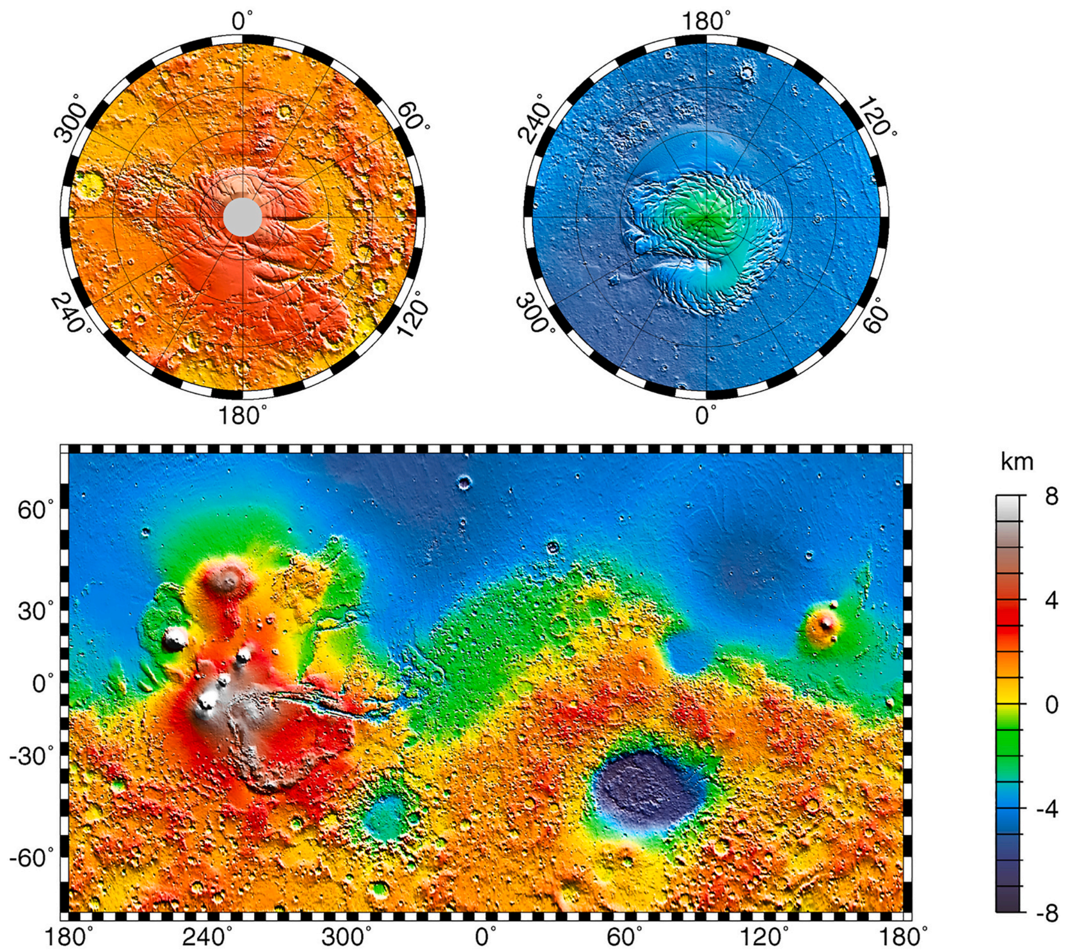

Fig. 1. These elevation maps from the Mars Global Surveyor instrument Mars Orbital Laser Altimeter show the hemispheric elevation difference and the difference in density of large craters between the northern and southern hemispheres (Smith et al., 2001a). At the top, the martian south pole is on the left; the martian north pole is on the right. JPL Photojournal PIA02031.

Titus et al., 2003; Byrne and Ingersoll, 2003; Bibring et al., 2004) and is considered to also be part of the residual cap above the underlying layered deposits. Below the residual caps, numerous layers of water ice mixed with dust, the "Polar Layered Deposits" (PLD), record past climate history (summarized in Smith et al., 2020). The NPRC covers most of the Northern PLD (NPLD), whereas only a small portion of the southern PLD (SPLD) is covered by the SPRC. In the north, the PLD exhibit the spectral signature of water ice mixed with dust (Calvin et al., 2009) but in the south the PLD lack the spectral signature of any ices (Doute et al., 2007; Langevin et al., 2006; Cartwright et al., 2022). Recent observations of the SPLD also suggest that large deposits of buried CO_2 ice, likely remnants of past low-obliquity periods, underly the location of the SPRC (Phillips et al., 2011; Alwarda and Smith, 2021; Buhler and Piqueux, 2021). Models of Mars' obliquity, eccentricity and longitude of perihelion combined with climate models suggest an age for the bulk NPLD of ~4 million years (Laskar et al., 2004; Levrard et al., 2007; Hvidberg et al., 2012), while the surface age is much younger (Herkenhoff and Plaut, 2000; Banks et al., 2010; Landis et al., 2016). The surface age of the SPLD is derived from crater counts to be 30–100 million years (Herkenhoff and Plaut, 2000; Koutnik et al., 2002) and stratigraphic studies suggest it may have accumulated over a 10–30 Myr period (Becerra et al., 2019).

The base of the NPLD is 5000 m lower than the planetary average elevation, with the top of the NPLD reaching -2500 m (Zuber et al., 1998). In contrast the bottom of the SPLD is at 1000 m above the global average with the peak at +4750 m (Smith et al., 2001a). This puts the two polar regions in different atmospheric pressure regimes with mean pressure >50% greater in the north, important for predicting atmospheric flow and volatile transport. The CO_2 frost point is approximately 143 K in the south and 150 K in the north, on average (Piqueux et al., 2023).

2.2. *The north polar erg*

The entire north polar residual cap is encircled by dark dunes, the north polar erg. Most of the dunes in this circumpolar sand sea are found poleward of 75° N, but in the sector from 270° E to 360° E the dunes reach to ~70° N (Fig. 2). Hayward (2011) identified three types of areas: 210,000 km^2 surface densely covered with dunes at 80–100%; 540,000 km^2 with medium surface coverage of 10–80%; and 90,000 km^2 widely scattered barchans with <10% surface coverage. The north polar erg accounts for ~75% of dune fields on Mars (Hayward et al., 2014). The average dune height in the north polar erg is 20–25 m with some barchans reaching ~50 m (summarized in Hayward, 2011). The dunes are composed of dark basaltic sand. Lighting on these dunes is key to understanding seasonal behavior, as shown in Section 4.

2.3. *Northern and southern mid-latitudes*

The mid-latitude region (~30°–65°) contains the edge of seasonal frost activity in both hemispheres and therefore offers opportunities to observe seasonal surface changes further into or throughout the fall and winter with better lighting conditions. While seasonal processes are more active poleward of ~70°, they are considerably harder to observe

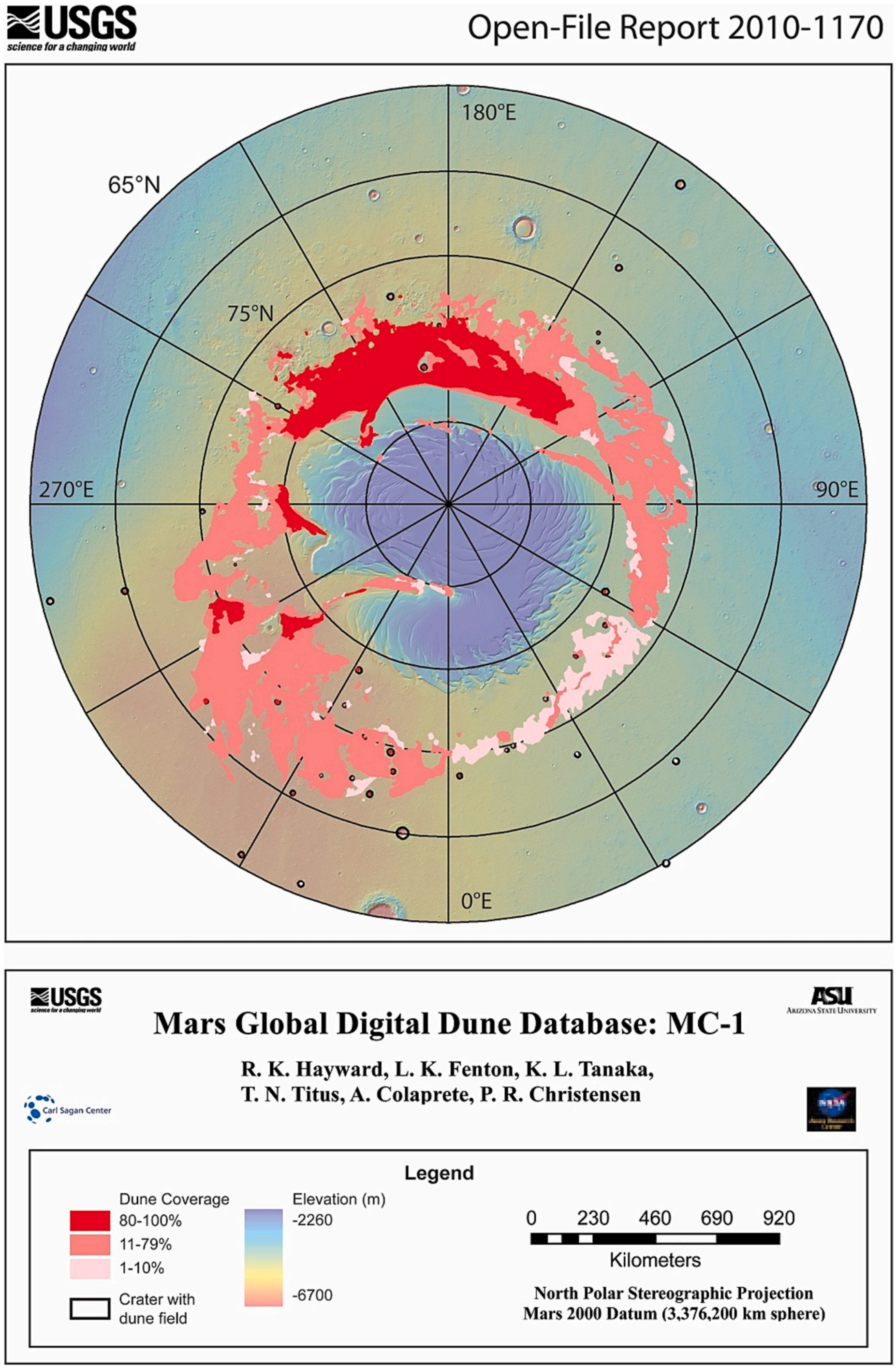

Fig. 2. This map of the north polar erg is from the USGS open file report 2010–1170 (Hayward et al., 2010). Dark red regions represent dense dune coverage of the surface; medium red is moderate dune coverage; and light pink regions contain scattered barchans. Yellow circles are craters with dunes. The latitude grid is 5 deg. (For interpretation of the references to colour in this figure legend, the reader is referred to the web version of this article.)

at high resolution (i.e., HiRISE or CTX) when the imagers have to contend with rapidly decreasing light levels and obscuration by the polar hood.

This has been especially true of seasonal activity in dune fields and crater environments. Most mid-latitude sand deposits in the northern hemisphere are small ($< \sim 10$ km^2) dune fields or sand sheets in craters, with several notably larger dune fields in Lyot, Lomonosov, and Moreux craters. Dunes have unique defrosting attributes because their geometry provides vastly different sun exposures on slopes depending on their orientation. Dunes in the mid-latitudes can be quite different in size and orientation than those of the north polar erg. For example, the mid-latitude dunes in the south can be very large compared to the north polar erg, e.g. the Russell crater mega-dune is 500 m high.

Gullies on dunes provide an interesting aspect of seasonal studies. Non-dune gullies with alcove-channel-apron morphology are observed on crater walls and other steep slopes in both hemispheres. Seasonal gully activity is common and allows further assessment of north-south differences (Dundas et al., 2019, 2022).

2.4. Equatorial region

CO_2 frost has been inferred to condense at night in the dusty equatorial regions (Piqueux et al., 2016) and on the tallest Tharsis volcanoes (Cushing and Titus, 2008), based on the analysis of surface nighttime temperatures and thermal modeling. Frost may have been detected in the early morning at high altitudes (Valantinas et al., 2023) in colour images from the Colour and Surface Stereo Imaging System (CaSSIS; Thomas et al., 2017). Other observations are very tenuous.

2.5. Southern high-latitude dunes

The latitude band from 60°S to 80°S accounts for 15% of Mars' dune fields (Hayward et al., 2014). Most dunes are found in craters or small fields, with latitudinally increasing signs of dune stabilization, likely due to induration by ground ice, poleward of 60°S (Fenton and Hayward, 2010; Banks et al., 2018). Morphology generally represents wind fields directly influenced by crater topography. Non-stabilized dunes show the classic stoss, brink, and slipface produced by saltation of cohesionless

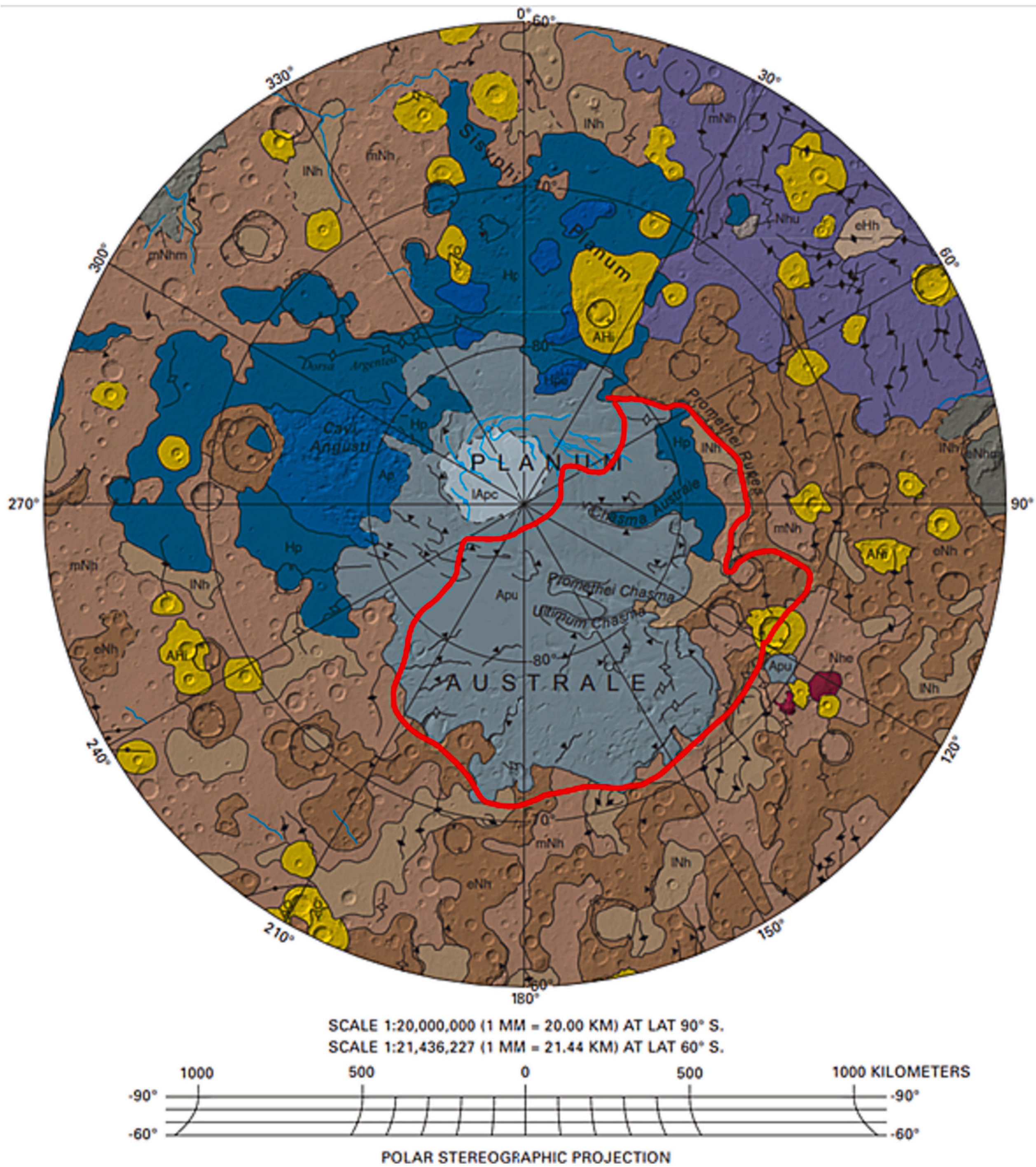

Fig. 3. This map of the south polar region shows the SPRC and SPLD units: the SPRC is very light grey, and the SPLD is a somewhat darker grey. The source of map is Tanaka et al., 2014. The red line marks the boundary of the cryptic contour terrain at L_s 222 (Titus et al., 2008). The actual outline varies slightly from one year to another depending on atmospheric conditions (Calvin et al., 2017). (For interpretation of the references to colour in this figure legend, the reader is referred to the web version of this article.)

sand. Dune fields displaying unclear/rounded structures may be more influenced by erosional or depositional factors than from winds. Often a 10-1000 m wide apron of dark sand surrounding the dunes merges with sand-covered interdunes (Fenton and Hayward, 2010), suggestive of slow and sporadic mobilization of only a thin sand cover over indurated and degraded duneforms. In particular, the "bullseye" dune fields are unique to the southern high latitudes, with concentric rings of rounded sand ridges within a steep walled crater (Fenton and Hayward, 2010). No dune fields are found poleward of 81°S (Fenton and Hayward, 2010).

2.6. South polar layered deposits and cryptic terrain

In contrast to the NPLD, which only reaches from 90° to 78° N, the SPLD extends to 72° S at some longitudes. This large extent is not symmetric around the geographic pole. The South Polar Residual Cap (SPRC) covers only a small fraction of the SPLD and is offset from the geographic south pole. The explanation for this asymmetry was found by Colaprete et al. (2005) to be due to the major topographic features in the southern hemisphere: the Hellas basin, Argyre basin, and the southernmost portion of the Tharsis rise. The presence of these features modulates south polar atmospheric circulation in the winter, resulting in two distinct climate regimes. The hemisphere west of Hellas, including the SPRC, is dominated by CO_2 snowfall in the winter; the hemisphere east of Hellas by CO_2 direct condensation (Colaprete et al., 2005; Hayne et al., 2014).

In the hemisphere east of Hellas, ~40°E to 220°E, a kidney-shaped region dubbed "cryptic terrain" is apparent in southern spring (Fig. 3). The cryptic region has generally low albedo in the spring but retains the cold temperatures of CO_2 ice (Kieffer et al., 2000). Coupled with observations of erosional features and dark fan-shaped surface deposits, this led to the Kieffer model for seasonal activity driven by sublimation from the bottom of translucent slab CO_2 ice (Kieffer et al., 2006, and discussed in Section 4.2). Meter-scale resolution images from HiRISE show a surface conformally coated with ice early in southern spring (Hansen et al., 2010). Observations by the Mars Express visible and infrared mineralogical mapping spectrometer OMEGA noted the disappearance of CO_2 ice spectral features after surface darkening occurs (Langevin et al., 2006, 2007b) but higher resolution views using CRISM and HiRISE note CO_2 ice features remain though they are muted by the dark fans (Pommerol et al., 2011).

A slab persists in Richardson crater (~72.6 S, 180.4 W) throughout the season (Andrieu et al., 2018). The thermal inertia is low upon defrosting (Putzig and Mellon, 2007), consistent with a covering of fine-grained dust.

3. Present-day seasonal drivers

Insolation is the dominant factor in the energy balance of a vapor-pressure-equilibrium climate, driving the seasonal behavior of the major volatile, CO_2 (Leighton and Murray, 1966). Controlling parameters include orbital eccentricity and obliquity, which determine the distribution of solar energy across the globe with season, as well as local slope and aspect. Mars' current obliquity is 25.192° (Allison and McEwen, 2000). At this obliquity the poles provide stable cold traps for seasonal ice in the fall and winter. In the spring the ice begins to sublimate, leading to a host of seasonal processes. The nature of the activity is described in Section 4.

Table 1
Mars' seasons are different durations due to the eccentricity of its orbit.

Start L_s	North	South	Duration in mean sols
0	Spring	Fall	193.30
90	Summer	Winter	178.64
180	Fall	Spring	142.70
270	Winter	Summer	153.95

The solar longitude of Mars in its orbit, L_s, is used to mark time and seasons, shown in Table 1. $L_s = 0°$ is the Mars vernal equinox, when the subsolar point crosses Mars' equator into the northern hemisphere. This marks the beginning of Mars' northern spring. Northern summer begins at $L_s = 90°$, the northern summer solstice. Southern spring starts at $L_s = 180°$; southern summer begins at $L_s = 270°$.

3.1. Mars' current orbit eccentricity and orientation

With an orbital eccentricity of 0.0934, Mars is ~20% further from the sun at aphelion compared to perihelion. At the top of the atmosphere the solar flux at normal incidence at aphelion is ~502 $Wm^{-2}\ s^{-1}$; at perihelion it is ~730 $Wm^{-2}\ s^{-1}$. Aphelion takes place at $L_s = 70.999°$, in northern spring approaching equinox. Perihelion is currently at ~$L_s = 250.999°$, late southern spring. The current orientation of the orbit ellipse leads to colder northern summers and shorter northern winters compared to the southern hemisphere.

The mean duration of a sol, one rotation of Mars, is 88,775.244 s (24.66 h). The number of mean sols per degree of L_s varies over the orbit, from 1.53 to 2.23 sols, due to the orbit eccentricity. Mars travels the fastest in its orbit at perihelion. The duration of southern spring, $L_s = 180°$ to 270°, is 142.7 sols. Days are relatively hot but the season passes quickly. The duration of northern spring, $L_s = 0$–90°, is 193.3 sols. The corresponding long southern fall allows more time for CO_2 to condense and accumulate. (See Table 1.)

The temperature of the ice and the pressure of the overlying atmosphere are linked in a vapor pressure equilibrium-controlled atmosphere, and how much ice sublimes or condenses is controlled by the energy balance of insolation, radiation of energy to space, and thermal conduction to the surface. As can be seen in Fig. 4, the dip in atmospheric pressure is greatest in northern summer, when the maximum fraction of the atmosphere has condensed in southern winter in the south polar region, due to its longer winter season. The dip in atmospheric pressure in northern winter is not as great as conversely the season is shorter.

The time available for CO_2 to condense in the southern hemisphere is appreciably longer than in the north. The peak mass of CO_2 ice is almost twice as high for southern winter compared to northern winter: ~3 × 10^{15} kg in the north vs almost 6 × 10^{15} kg in the south, integrated poleward of 60° (Kelly et al., 2006; Titus et al., 2008; Schmidt et al., 2010). For an annual average atmospheric mass of 2.17 × 10^{16} kg, calculated from the mean global surface pressure of 5.6 mbar, that represents ~14% peak decrease due to northern frost and a 22% decrease due to southern frost. The average latitudinal boundary of the seasonal CO_2 cap ice has been identified at ~50° N and ~ 48° S with equivalent maximum areas of ~1.8 × 10^7 km^2 (north) and ~ 1.9 × 10^7 km^2 (south), with modest longitudinal variations (Piqueux et al., 2015a).

On cold pole-facing slopes, seasonal CO_2 forms at lower latitudes. Detections of CO_2 frost patches from OMEGA and CRISM reach as far equatorward as ~35°S (Vincendon et al., 2010). Small traces of frost with uncertain composition have been observed on such slopes closer to the equator (Schorghofer and Edgett, 2006; Dundas et al., 2019).

In addition to geometric considerations of obliquity and the elliptical orbit, the different elevations of the two hemispheres lead to differences in surface pressure, which influence ice temperature, thickness and duration of the seasonal ice cover. The longitude of perihelion is also important in the southern hemisphere. Higher pressure in the northern polar areas leads to warmer CO_2 frost and faster infrared radiation to space. At face value this should enable frost to condense faster on the northern polar surface; however, this effect is overshadowed by the shorter polar night and role of snowfall, providing contaminants.

3.2. Seasonal variability in recent history

Mars' orbital parameters and obliquity are not static. Seasons have

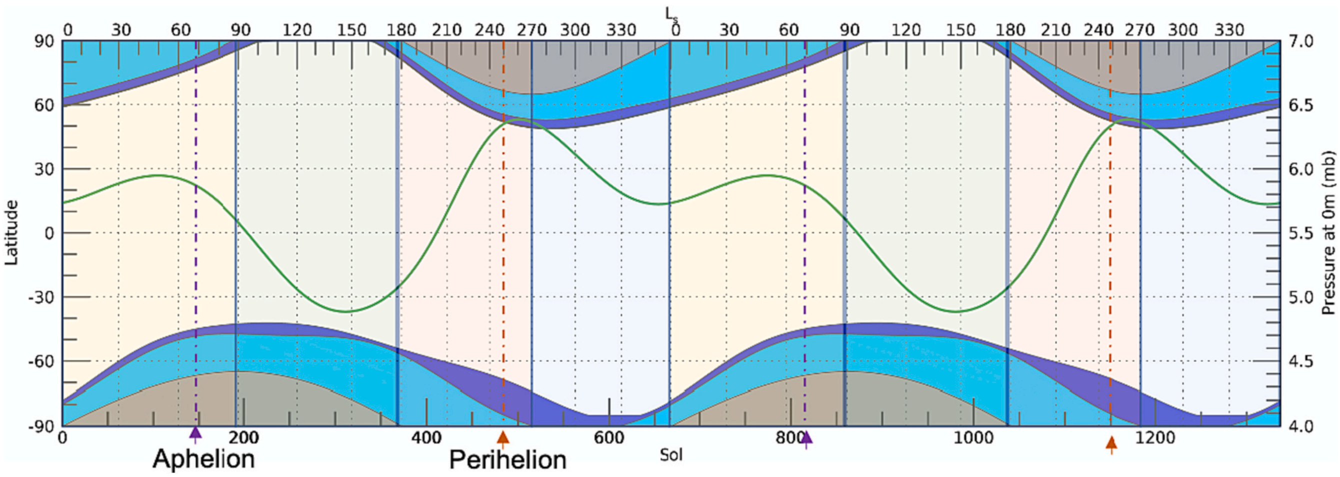

Fig. 4. The pressure cycle for two Mars years (green, right axis) shows two pressure dips per year. The first is a large dip in northern summer as CO_2 condenses and forms the southern seasonal cap. The second, more minor dip is in late southern summer as the northern winter cap forms. The peak atmospheric pressure roughly coincides with perihelion. Colour shading shows northern spring (yellow), summer (green), fall (light orange), and winter (blue). The grey shading shows the extent of polar night in latitude (left axis). Light blue and dark blue show the minimum and maximum latitudinal extents of seasonal frost, respectively (Titus, 2005), also known as the inner and outer crocus line. The pressure curve is from Tillman et al. (1993). (For interpretation of the references to colour in this figure legend, the reader is referred to the web version of this article.)

varied over recent geologic time. Obliquity has oscillated from lows of 15^o to highs up to 35^o in the last 2 Myr, with even greater excursions, likely to over 60^o, in the more distant past (Laskar et al., 2004). The orbit eccentricity cycle is ~95,000 years and has varied from ~0 to 0.12 over millions of years (Laskar et al., 2004). Precession of the argument of perihelion over the full 360 ^{o} takes ~51,000 years. This will affect the latitudinal extent of the north-south differences. These climatic cycles have profound effects on the transport and cold traps of volatiles seasonally, and are thought to be reflected in the structure and deposits in the PLD (Murray et al., 1973; Laskar et al., 2002). To describe these effects is beyond the scope of this paper, however linking current seasonal cycles to current depositional and erosional patterns in the current climate is a major topic for future studies of Mars' climate history. Insights into the current seasonal asymmetry and its effects support efforts to understand the long-term outcomes of these variations.

4. Northern vs. southern seasonal activity

In Section 4 we review the seasonal processes that have been studied with MRO's payload. In contrast to Sections 2 and 3, which are static when focusing on only the current timeframe, Section 4 examines the active seasonal processes. Much of this material has been reported for either north or south, but this paper compares the two. We begin with the seasonal meteorology in Section 4.1. Kieffer's model is described in 4.2.1 to 4.2.3, along with the nature of solid CO_2 the model relies on. Sublimation processes are compared in two categories—those that erode the surface with basal sublimation under the seasonal ice via Kieffer's model, 4.2.4 to 4.2.6, and those that erode the surface with seasonally driven mass wasting in 4.3.1 to 4.3.3. In Section 4.4 we compare the processes latitudinally on dunes.

4.1. Meteorology

Both polar regions are dominated by wintertime circumpolar jets that form a boundary between the meridional overturning circulation (Hadley cell) and the polar vortex. Cold air remains isolated inside the polar vortex, which roughly coincides with the boundary of polar night, extending to ~65° latitude at mid-winter. Poleward transport of water vapor and dust is inhibited across this boundary, and the average atmospheric column in the polar winter is extremely dry and relatively clear of dust. However, especially in the north, dust and water injection occurs through sporadic disruptions and weakening of the vortex, driven by dust storms and subsequent atmospheric heating (Alsaeed and Hayne, 2022). During these periods, and most pronounced in the perihelion dusty season (northern winter), MCS observes rapid changes in the temperature structure, size, and cloudiness over the poles.

Carbon dioxide snowfall (Hayne et al., 2014) is common in both polar regions throughout their winter seasons (Widmer et al., 2023). Prior to MRO, models and a limited set of infrared observations suggested the presence of optically thick clouds and possibly snow (Forget et al., 1995; Colaprete and Toon, 2002), but it was challenging to distinguish snowfall from surface CO_2 frost formation (Titus et al., 2001). Early observations with MCS confirmed the presence of massive CO_2 clouds extending from the surface to ~30 km altitude at the south pole (McCleese et al., 2008). Further limb-sounding observations with MCS linked these clouds to widespread snow accumulation within the polar night (Hayne et al., 2012), consistent with up to ~20% of the total column mass of the seasonal CO_2 cap contributed by snowfall (Hayne et al., 2014). The snow clouds are dominated by ~10–100 μm CO_2 ice particles, likely containing much smaller amounts of water ice and dust as condensation nuclei.

Given that the northern winter coincides with the perihelion dust storm season and a higher mean dust optical depth, the north polar seasonal ice deposits are expected to contain a greater concentration of dust in relation to CO_2 and H_2O ices. This north/south difference is apparent in both the surface deposits (lower albedo and emissivity in the north) and in the patterns of clouds and precipitation. A study using MCS surface emission spectra and atmospheric aerosol retrievals showed the stark contrast between the north and south poles: snowfall is much more frequent and intense in the north, as are both the dust and water ice abundances (Gary-Bicas et al., 2020). Analysis and modeling of the MCS data indicated that north-polar snowfall deposits roughly 10× as much mass of both CO_2 and H_2O relative to direct surface accumulation compared to the south. Scavenging of H_2O ice particles by CO_2 snowfall thus accounts for a minimum of ~10^9–10^{10} kg of water in the north, and ~ 10^8–10^9 kg in the south, each winter (Alsaeed and Hayne, 2022).

Spatial patterns of CO_2 accumulation and snowfall are also distinct between the two poles. Colaprete et al. (2005) found that the high albedo and long-term stability of the SPRC may be related to enhanced snowfall occurring in the longitude quadrant − 90° to 0°E, driven by a topographically forced stationary wave set up by Hellas and Argyre basins. Furthermore, the opposite quadrant contains the Cryptic region, where snowfall is less common and instead slab ice is dominant (Titus et al., 2001). The MCS limb sounding and surface emissivity observations are generally consistent with these patterns, although it is the north polar region that exhibits a stronger zonal wavenumber-2 variation in snowfall (cf. Waugh et al., 2016; Gary-Bicas et al., 2020; Alsaeed et al., 2022). In the south polar region, snowstorms appear to be driven much more by topography, notably at the ~100-km horizontal scale. This is likely a consequence of the much higher cooling (and precipitation) rates possible through orographic lifting and adiabatic cooling given the rougher southern terrain, compared to infrared emission to space (Forget et al., 1998; Colaprete et al., 2003). In short, the south polar region simply has greater topographic roughness at the relevant spatial scales.

Large-scale patterns of frost and snow accumulation at both poles are remarkably repeatable from year to year (Byrne et al., 2008; Schmidt et al., 2009; Piqueux et al., 2015a; Calvin et al., 2017; Acharya et al., 2023). Interannual variability of the climate driven by regional and even planet-encircling dust storms appears to only affect water ice accumulation at small (<10 km) spatial scales in isolated regions. However, the more dramatic effects of global dust storms are apparently felt by the seasonal caps, which show accelerated retreat during several months following the decay of the dust storms (Piqueux et al., 2015a). Intriguingly, lower-than-expected atmospheric pressure values acquired by the InSight lander could be explained by a larger-than-usual North seasonal cap in response to the MY34 global dust event, (Lange et al., 2022) and numerical modeling confirms that increased dust loading may regionally increase the size of the North seasonal cap (Zhao et al., 2021). The system quickly resets, with no effects observed on the extent of the seasonal caps just half a Mars year later. Interannual variations in snowfall appear to be more pronounced: during MY 29–35, Alsaeed et al. (2022) found variations of ~50% in snow accumulation in the south, and ~ 25% in the north. These interannual variations also appear to be linked to the dust cycle (Alsaeed et al., 2022), but the mechanism remains unclear.

4.2. Seasonal surface activity

Seasonal sublimation of CO_2 ice is the dominant erosive force on Mars today (Piqueux and Christensen, 2008; Diniega et al., 2021). Processes sculpting the surface can be divided into two categories: 1) erosion of the substrate from basal sublimation below the seasonal ice and 2) seasonally-triggered mass wasting events.

In the first process, escaping gas entrains particles from the ground below the seasonal ice layer and scours channels in both the northern and southern hemispheres. A wide variety of configurations of channels have been observed—the escaping CO_2 gas will find the path of least resistance. This is described in Sections 4.2.1 to 4.2.6. In the second process, the timing of the formation of gullies and alcoves on dunes has been shown to be seasonal (summarized in Diniega et al., 2021). Linear gullies exhibit symptoms of both, but are categorized as mass wasting events. These processes are described in Sections 4.3.

4.2.1. Kieffer model

The seasonal processes associated with sublimation of the seasonal CO_2 ice are well-described by the “Kieffer model” (Kieffer et al., 2006; Kieffer, 2007). The Kieffer model postulates that energy from insolation penetrating impermeable translucent ice, combined with residual subsurface heat, causes the seasonal CO_2 ice to sublimate at the bottom of the seasonal slab. Gas is trapped under pressure until a rupture occurs. Escaping gas entrains material from the ground below the seasonal ice layer as it rushes to the vent created at the rupture. The particles are carried up into the ambient atmosphere, then settle in fan-shaped deposits on the surface of the seasonal ice in a direction determined by the local wind (Kieffer et al., 2000; Piqueux et al., 2003; Kieffer et al., 2006; Kieffer, 2007; Aharonson et al., 2004). The Kieffer model was developed to describe the southern spring seasonal processes and specifically the appearance of spots, fans and development of araneiform (“spider”-like radially organized channels) terrain on the SPLD. The model, which aimed to describe features in MOC images, has been bolstered and only slightly modified by detailed examination with the high spatial and temporal resolution of HiRISE images (Hansen et al., 2010; Thomas et al., 2010; Portyankina et al., 2010; Mc Keown et al., 2023). A thermal wave from the ground was hypothesized by Aharonson et al. (2004a), but later found to be limited by Pilorget et al. (2011).

Although originally applied only in the south, the model can also be applied to the seasonal processes in the north polar region, on the dunes of the north polar erg. HiRISE images acquired over an entire northern spring suggest that the same basic model, modified for application to the northern dunes, applies as shown in Fig. 5 (Hansen et al., 2013; Portyankina et al., 2012, 2013). Ruptures occur at weak spots on the dune: cracks along the brink, outbreaks around the dune margin, and polygonal cracks in the relatively flat sheet of ice on the dune stoss slope.

4.2.2. The nature of CO_2 ice

One of the requirements of Kieffer’s model for creation of jets is that the seasonal CO_2 ice is in the form of a translucent, impermeable slab, as a slab layer is needed a) for sunlight to penetrate through it to the ground, and b) to contain gas and allow rising pressure held underneath it so that when it inevitably breaks through the ice, it creates pressurized jets. Only if the gas flow underneath the ice layer is pressurized would it be able to erode the semi-frozen polar substrate into visible tributaries of araneiforms, furrows, and dendritic troughs (summarized in Mc Keown et al., 2023). There are indirect observational indications that CO_2 ice observed in the spring is not a snow-like permeable layer but rather a solid dense slab that breaks in a typical pattern of linear cracks (Portyankina et al., 2012).

Another confirmation comes from laboratory experiments: under specific martian conditions CO_2 deposits form much more readily into a slab than as unconsolidated crystalline ice (Portyankina et al., 2019; Mc Keown et al., 2021). To form unconsolidated crystals requires crossing of the phase transition curve at either much colder and rarified or warmer and pressurized conditions than is expected to be found during a martian winter. In addition, the laboratory studies also showed that even if CO_2 first deposits as snow, when exposed to martian polar conditions, the ice will densify into a slab. This slab is less transparent than one produced through direct deposition, but will still follow the Kieffer model as it is translucent enough to the visible spectral range of sunlight to create a solid-state greenhouse effect.

When comparing seasonal processes in southern and northern hemispheres, differences in the “quality” (strength, transparency) of slab ice can be connected to all the other differences between the hemispheres. Ice slab quality depends on:

a) the length of winter (or the season that allows CO_2 deposition), because with more time a thicker slab will be created and more snow can densify into a slab. In mid-latitudes, for example, CO_2 can only deposit a thin and discontinuous layer, which is easily broken by rising pressure and thus would lack the high-pressure erosional sub-ice flow needed to excavate troughs;
b) the specific pressure-temperature (P-T) conditions during deposition, because different types of ice tend to form at colder and warmer conditions than usual martian polar conditions. The southern hemisphere is on the low P-T limit of slab deposition, while the northern is on the higher end due to their difference in elevation (see Portyankina et al., 2019, Fig. 8). How exactly this translates into ice quality is uncertain at this time;
c) the presence of contamination, because ice deposited simultaneously with dust or water ice is more brittle and less transparent. While there is a mechanism for removing dust contamination from inside the slab ice (described in the original Kieffer model, see Kieffer, 2007), there is no known process that removes water ice contamination. The northern hemisphere has more water vapor and it shows

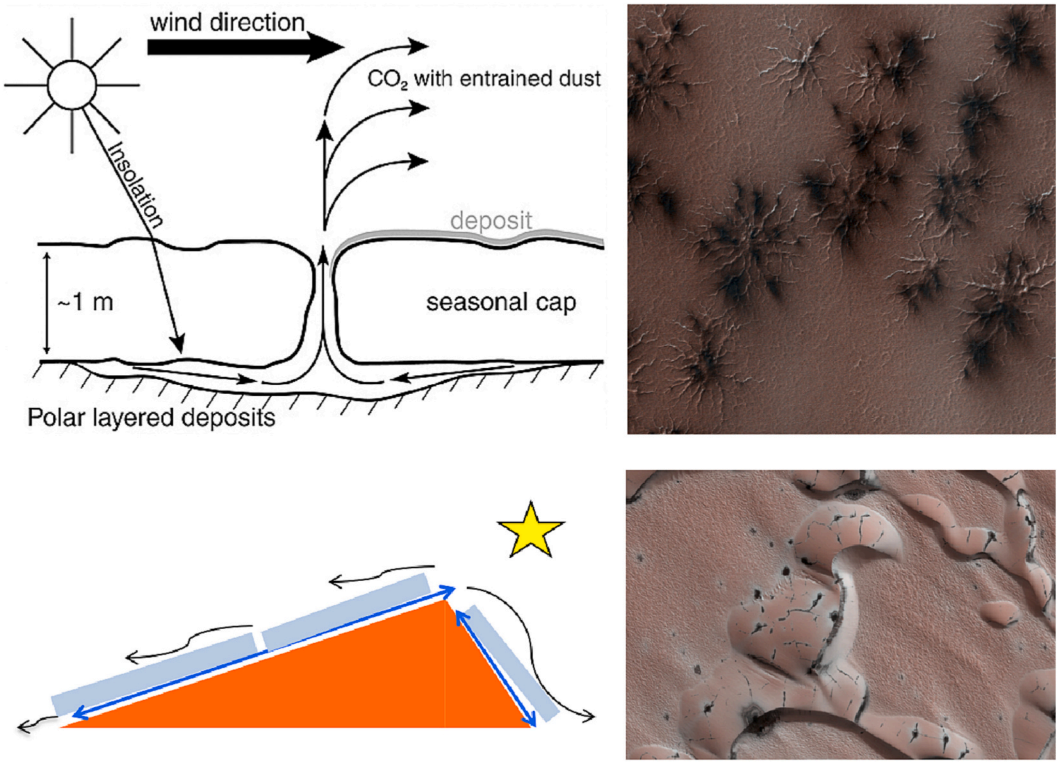

Fig. 5. Kieffer's model is illustrated for the south (top panel) and north (bottom panel). The upper left diagram is adapted from Piqueux et al. (2003). The upper right image is a cutout from ESP_011420_0930, taken at latitude / longitude 87°S / 127.27°E, at L_s 184.3°. At the time of image acquisition, at this latitude, seasonal ice is ~ 0.7 m thick (Kelly et al., 2006) and fans of material have deposited after jetting from ruptures, covering the surface near their vents along araneiform troughs. The lower left diagram shows the Kieffer model applied to the northern dunes (Hansen et al., 2013). Three weak spots (black arrows) are conducive to rupture: the dune-surface interface, cracks along the dune brink, and polygonal cracking of the sheet of ice covering the stoss side of the dune. The image in the lower right is a cutout from ESP_025042_2650, latitude / longitude 84.7°N / 0.7°E, at L_s = 36.6°, when the seasonal ice is ~ 0.5 m thick. Dark material from the dark dune has emerged from all 3 types of weak spots.

up in seasonal deposition patterns, with a micron-thin water ice layer detected latitudinally-below the edge of the seasonal CO_2 layer. Water frost is left behind as a lag deposit, after the seasonal CO_2 sublimes (Wagstaff et al., 2008). Almost no water ice is observed in the south (Langevin et al., 2007b).

Spring activity in the north and south polar regions show similar features, which demonstrates that there must be similar processes happening, including deposition and then sublimation of slab CO_2 ice. The details of the process and substrate are what create the variety of the observed features.

4.2.3. *Thickness of the seasonal CO_2 ice layer*

A number of authors have estimated the amount of condensed CO_2 and thickness of the seasonal ice layer as a function of time and latitude. The first 3 columns of Table 2 use the data from Mars Odyssey's Gamma Ray Spectrometer (GRS), reported in Kelly et al. (2006). Maximum column densities are approximate as they are estimated from the plots in Fig. 3 of Kelly et al. (2006). The 4th, 5th, and 6th columns are the possible end members for computing the thickness of the layer: slab CO_2 ice in column 4, average CO_2 ice density estimated from MOLA surface altitude measurements (Smith et al., 2001b) in column 5, and density derived from surface altitude changes in MOLA data from groundtrack cross-over points (Aharonson et al., 2004) in column 6. Variable density was hypothesized by Matsuo and Heki (2009) to explain MGS gravity

Table 2
Seasonal ice layer thickness. See text above for source of data.

L_s at maximum column density	Latitude of maximum column density	Approximate maximum column density (gm/cm^2)	Max thickness if density = 1.6 g/cm^3 (cm)	Max thickness if density = 0.92 g/cm^3 (Smith et al., 2001b) (cm)	Max thickness if density = 0.5 g/cm^3 (Aharonson et al., 2004) (cm)
North					
320	60°	10	6	11	20
340	67.5°	25	16	27	50
350	75°	45	28	49	90
10	82.5°	68	43	74	136
South					
145	−60°	30	19	33	60
160	−67.5°	45	28	49	90
185	−75°	62	39	67	124
190	−82.5°	75	47	82	150

field measurements. The best fit to their data is represented by a layer of CO_2 that increases in density as the season goes on, such that the layer would start at the low end of the density range and over the course of the winter density increase to as high as 1.5 g/cm^3. The L_s of frost condensation varies with latitude. Actual densities are also related to whether the CO_2 condenses directly or as snowfall (Mount and Titus, 2015). Most recently (not in table) Xiao et al. (2022a, 2022b) have estimated the thickness of the ice from MOLA profiles for both the northern and southern cap, and reach values even higher than the numbers in the last column. This suggests another hemispheric difference–the longer winter in the south leads to denser, less porous ice.

4.2.4. Onset and development of seasonal sublimation

In both the northern and the southern hemispheres the first places to show seasonal fans, indicative of the presence of a rupture in the ice, are on rough terrain where an exposed lip or point is the first to be exposed to sunlight. In the north, the rough surface between the dunes commonly shows the earliest outbreaks, shown in Fig. 6. On the dunes themselves, early sublimation spots commonly occur along the dune brink (Hansen et al., 2013).

In the south the equator-facing lip of araneiform troughs is often the first place to show rupture(s) as shown in Fig. 7, taken at L_s 188.9. At this early time in the season the entire area is covered by CO_2 ice. This may explain why araneiform troughs are wide and shallow - the main erosion is from the side, not the floor of the trough. Troughs are rarely over 1 m deep but are often many meters wide (Hansen et al., 2010).

4.2.5. Seasonal activity throughout spring as seasonal ice sublimates

As indicators of when and where ice ruptures occur, spots and fans provide detailed information regarding the course of sublimation-driven activity. The number and timing of gas jets emanating from under seasonal ice will depend on the translucency of the ice (which determines the rate of sublimation on the bottom by affecting the amount of insolation that penetrates), the subsurface properties, and the thickness and permeability of the seasonal ice layer, since a rupture is needed for the gas to escape (Kieffer, 2007). The spacing of fans gives a sense of the capacity for gas storage under the ice (soil porosity, permeability) as well as the strength of the overlying slab of ice (Hao et al., 2020). The length of the fans depends on several factors: strength of the wind, velocity of gas leaving vent, and the local topography (Thomas et al., 2011; Portyankina et al., 2022). The orientation of the fans reflects the direction of the ambient wind at the time of the eruption. If there is no wind, the particles fall back down and form dark blotches around the vent.

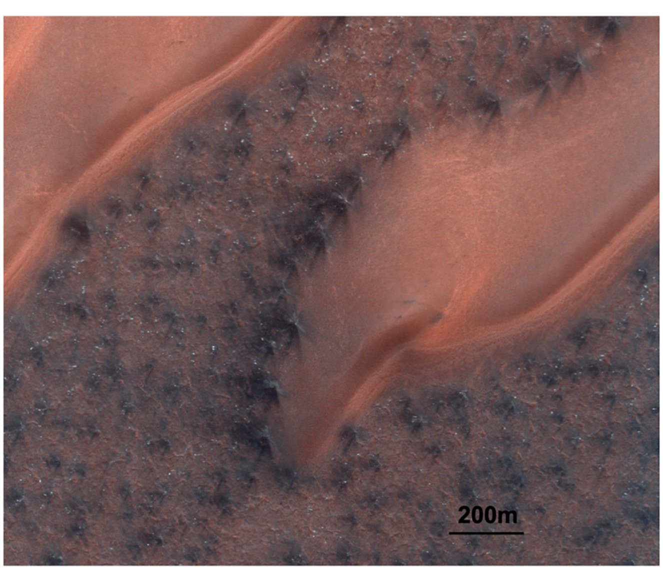

Fig. 6. ESP_024247_2600 was taken at $L_s = 7.5^\circ$ in an area known informally as Arrakis at 80°N / 122°E. The rough surface between the dunes is the first to show seasonal fans where the ice has broken.

Examples of typical spring sequences are shown in Figs. 8 and 9. In the northern hemisphere (Fig. 8), dark sand emerges from the weak spots on the brink and around the perimeter of the dunes, and from polygonal cracks on the stoss side of the dunes. On the dunes the direction of the sand flow is mostly dependent on the topography, sliding downhill, but late spring winds may blow the sand in other directions. Eventually the dark sand merges into apparent ice-free areas on the dunes (Hansen et al., 2013). A typical spring sequence in the southern hemisphere is shown in Fig. 9 (Hansen et al., 2010). Fans from jets emerge early in spring. With time, particles sink into the ice, leaving behind grey vestiges of fans. Fans may emerge from the same location multiple times in a single season.

4.2.6. Erosion by basal sublimation

The nature and timescale for erosion of the surface by basal sublimation is controlled by the friability of surface material. This erosion manifests as shallow channels carved into the substrate, remaining after the frost has sublimated. Such erosion spans a range of sizes and timescales of retention, forming furrows, dendritic troughs, and the "spiders" in araneiform terrain (as summarized in Mc Keown et al., 2023).

On the dunes of the north polar erg, shallow and ~ meter-wide furrows are formed every spring as gas escapes to ruptures (Bourke and Cranford, 2011; Hansen et al., 2013; Diniega et al., 2021; Mc Keown et al., 2023). These furrows extend tens of meters over the dune slope and generally only last one year: summer and fall wind-driven sand transport erases the furrows and during the next spring new ones appear. Some may appear in the same place as a furrow formed during a previous winter, if the weak spot for the seasonal rupture is in the same place. The furrows do not grow visibly wider or deeper after their initial appearance.

In the southern hemisphere, dendritic troughs have been observed to grow, enduring from one year to the next (Portyankina et al., 2017) and are hypothesized to eventually grow into the larger araneiform features. These troughs are similar in size to furrows but persist and extend, developing new tributaries each year. In these locations the channels are being carved into the surface in regions adjacent to dunes, suggesting that sand abrasion helps with the scouring of surface material.

On the SPLD, escaping gas has been proposed to have carved radially-organized spider-like channels in the surface under seasonal ice, forming araneiform terrain (Piqueux et al., 2003). No changes within these spiders have been detected yet in HiRISE images, but the expected timescale for erosion of the SPLD is difficult to determine. A minimum of 10^4 years for feature formation has been hypothesized based on the volume of a "spider" and the estimated volume of dust excavated on a yearly basis (Piqueux and Christensen, 2008). In addition, a citizen science project was successful at finding spiders in CTX images that are not on regions mapped as SPLD, and the locations suggest that surface material properties are similar to those found in the SPLD and conducive to excavation (Schwamb et al., 2018).

Although seasonal fans are observed in the northern hemisphere on non-dune surfaces, the substrate has not been eroded into well-developed araneiform terrain, suggesting the presence of more cemented and/or coarser-grained surface material.

4.3. Gullies and alcoves on dunes from seasonally-triggered mass wasting

Seasonal activity controlled by the condensation and sublimation of CO_2 is thought to drive the formation of new alcoves on northern dunes (Hansen et al., 2011, 2013; Diniega et al., 2021), generation and extension of linear gullies with pits at the end (Diniega et al., 2013) and a variety of changes in gullies on dunes and non-dune slopes (Diniega et al., 2010; Dundas et al., 2012, 2015, 2019, 2022).

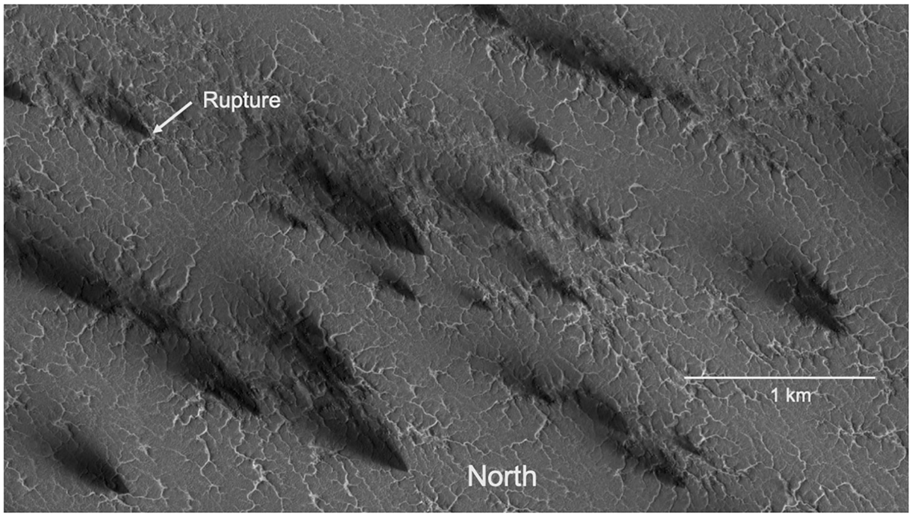

Fig. 7. This cutout shows ruptures often facing the equatorward (north) side of the araneiform channels. Image ESP_55604_0930 was taken at latitude / longitude − 86.89°S / 170.5°E, at $L_s = 188.9°$ when the entire area is covered by CO_2 ice.

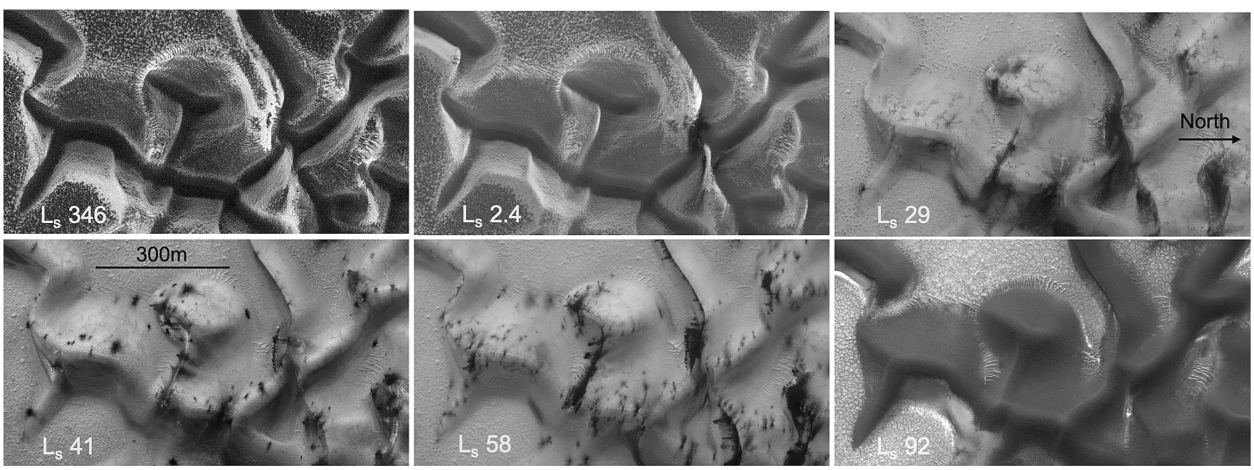

Fig. 8. These cutouts are from images of a seasonal monitoring site dubbed Del Mar at 79.8°N / 234.3°E. The first image is entirely covered with a layer of seasonal CO_2 ice and does not yet show the beginning of seasonal activity (contrast has been stretched to show topography, due to low light levels). By the time of the third image the seasonal cracks and outbreaks along the brink and dune-surface have started to emerge. In the final image only a few patches of seasonal ice remain. These cutouts are from (left to right) ESP_067786_2600, ESP_068195_2600, ESP_068921_2600, ESP_069264_2600, ESP_069739_2600, and ESP_070741_2600.

4.3.1. *Alcoves on dunes*

New alcoves (and related aprons) have been observed to form on north polar (Hansen et al., 2011, 2013; Diniega et al., 2021) and mid-latitude dunes (Widmer and Diniega, 2019). See Fig. 10. HiRISE image sequences over the course of a Mars year show that the formation of these alcoves is confined to late fall / early winter (Pasquon et al., 2016, 2019; Diniega et al., 2021), but the exact mechanism is still being explored. Initially Hayne et al. (2014) explored the hypothesis that CO_2 snowfall could cause slope failure but more years of targeted data acquisition showed that such an effect was possible but further moderated. In particular, an early snowfall after the first frost condensation may induce the early avalanching that carves out many of the largest alcoves (Hansen et al., 2018). Sublimation of seasonal frost may increase the size of the new alcove in the spring, especially as sublimation spots seem to preferentially appear within the new large alcoves (Fig. 10).

4.3.2. *Gullies*

Similar in form to the dune alcoves, but often with a channel connecting the alcove and apron, gullies are common landforms found on steep sandy and rocky slopes in the mid-latitudes in both hemispheres, although significantly more numerous in the south (Harrison et al., 2015). Unlike the northern dune alcoves, gullies on dune or rocky slopes may reactivate over multiple martian winters, forming new alcoves/channels/aprons or extending any of these features (Dundas et al., 2012). Extensive monitoring by HiRISE has demonstrated that gully activity correlates with the presence and springtime sublimation of CO_2 frost (Diniega et al., 2010; Dundas et al., 2012, 2015, 2019; Vincendon, 2015). Although the triggering mechanism for this activity may in some cases be the same as the Kieffer mechanism for defrosting spots and flows (Pilorget and Forget, 2015), a variety of other factors may cause failure on steep slopes, and defrosting spots are only rarely observed (Dundas et al., 2019). The CO_2 frost is thought to play a critical role in the flow process as its vaporization can fluidize the avalanching rocky debris, making the downslope movement behave more like a wet flow than dry mass wasting (Hoffman, 2002; Dundas et al., 2019; De Haas et al., 2019).

Before-and-after imaging, primarily using HiRISE, has demonstrated widespread gully activity with a marked hemispheric asymmetry. In the southern hemisphere, 22% of monitoring sites have had gully flows, while only 8% of those in the north have been similarly active (Dundas

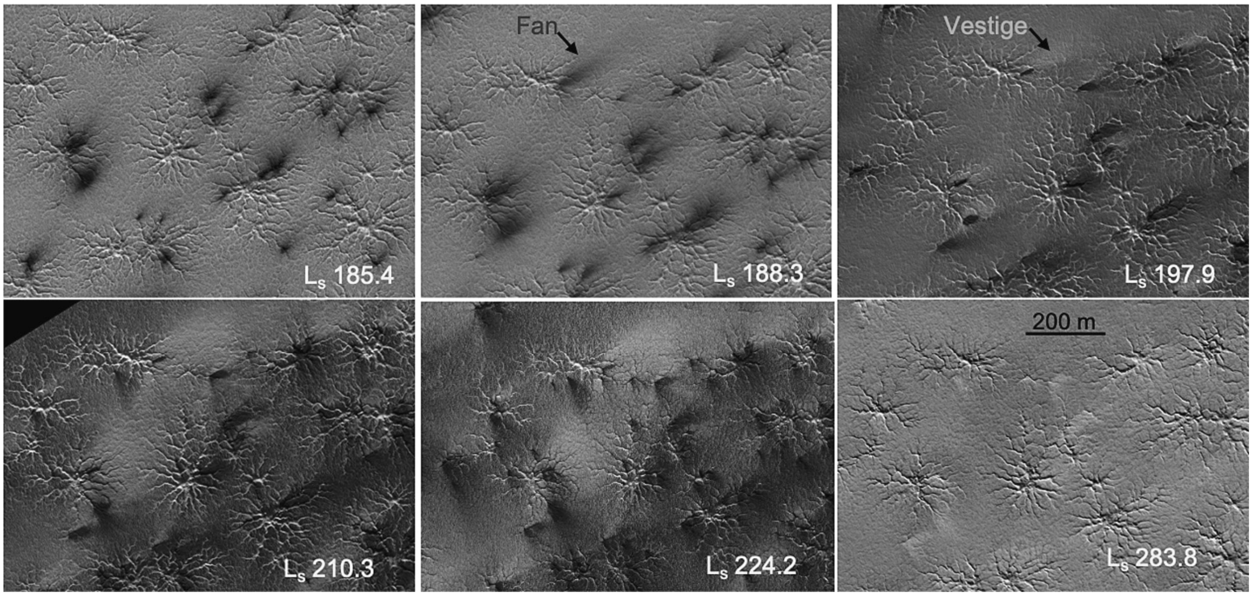

Fig. 9. These cutouts are from images of a seasonal monitoring site dubbed Bilbao at 87°S / 127.3°E. Sunlight is coming from the top of the images. The first image, taken at $L_s = 185.4°$, shows fans from early ruptures deposited on a seasonal ice layer ~ 0.5 m thick. As time goes on some of the particulates sink into the ice, leaving behind a grey vestige of the fan as can be seen in the third panel, taken at $L_s = 197.9°$. By $L_s = 224°$ bare areas are beginning to emerge. In the final image the seasonal ice is gone. These cutouts are from (left to right) ESP_073161_0930, ESP_073227_0930, ESP_073438_0930, ESP_073702_0930, ESP_073992_0930, and ESP_075205_0930.

et al., 2022). Additionally, activity extends to the lower latitude limits of well-defined gullies in the south, but the lowest-latitude gullies in the north have not yet been observed to be active (Dundas et al., 2022). These differences in amount and activity extent have been attributed to the longer winter and more extensive frost in the southern hemisphere, and should reverse over tens of thousands of years (Dundas et al., 2022). Thus, gullies may reflect the effects of frost processes integrated over longer timescales than those recorded by other landforms. It remains debated whether liquid water also played a role in past gully evolution (e.g., Conway et al., 2019) but CO_2 frost processes alone may be sufficient (Dundas et al., 2019, 2022).

4.3.3. Linear gullies on dunes

Features called "linear gullies" are also found on the southern mid-latitude dunes and sandy slopes, and are thought to be created when CO_2 ice blocks break from the seasonal frost layer and slide down a frost-free sandy slope (Diniega et al., 2013; Dinwiddie and Titus, 2021). As the CO_2 ice block comes into contact with the warmer sand, the base of the block sublimates, allowing the ice block to coast down slope, carving out a very shallow track in its wake. The source of sinuosity for some of these features is still debated, but may be due to activity repeated through many martian winters, with ice blocks forming in later winters bouncing off of the levees created by early blocks. The terminal pits are formed when the latest block comes to rest and sublimates in place, kicking out sand under and around it (Diniega et al., 2013). Blocks of ice have been observed near the terminus of linear gullies in late spring (Dundas et al., 2012; Diniega et al., 2013; Mc Keown et al., 2017).

The generation of linear gullies is likely due to a combination of surface and frost properties: the slope must be of sufficient length for a track to be carved and alcoves need to remain shadowed even after the area downslope has defrosted, so that the detached ice block can slide down a warm slope (Diniega et al., 2013). The surface must be sandy enough for a track to be left, and the sand must not be active enough to erase the forming tracks. Further, the temperature difference between the substrate and ice block must be large enough that a vapor layer can form under the block. Finally, the layer of seasonal CO_2 frost must be thick enough to form coherent ice slabs that fracture, forming ice blocks of sufficient strength to move down the slope. The grain size on martian sands is ~210 um, a medium to coarse sand (Edgett and Christensen, 1991). Fig. 11 shows a segment of Russell crater dunes with ice in the dune alcoves, and pits at the end of linear gullies.

4.4. Latitudinal comparison of dunes

Observations of seasonal processes on dunes provide us with the most direct north-south seasonal comparisons as, with dunes, the base under the seasonal ice is a consistent material. Dunes are composed of sand grains, which on Mars are generally the size of fine sand, 60–200 μm diameter. However, there are relevant characteristics of the dunes and dune field topographies that differ, such as the dune sizes and morphologies, that will influence seasonal properties. The interiors of some dunes may be more cemented by ice. Some dune fields contain more variety in their orientations: dunes in the north polar erg have consistent orientations, relative to the pole, as their orientation is primarily set by the winds in the north polar vortex while dunes in craters will be influenced by the local wind field. In spite of these caveats, we focus on the differences in the seasonal frost formation and sublimation processes as a function of latitude. Fig. 12 shows the sublimation process on dunes in the north polar erg (a), dunes at northern (b) and southern (c) mid-latitudes, and dunes in the south polar region (d) at a time when each field has an estimated coverage of ~10 cm of ice. As shown in Fig. 12, the quality (strength and transparency) of the CO_2 ice prevails in determining the nature of the sublimation process.

4.4.1. Northern high-latitude dunes

Based on the appearance of fans and spots, the seasonal CO_2 ice layer forming over the north polar dunes seems to have high strength by the end of winter. The ice first ruptures only at expected weak spots at the brink of the dune or along the dune margins, where the slope changes rapidly and thermal gradients are likely to be larger given a compositional/thermal inertia difference between the substrate and dune sand. These ruptures, especially from the brinks, seem to involve significant excavation of sediment as they often feed into flows. Later ruptures occur over the dune stoss slope (Figs. 5 and 8). The first stoss-slope sublimation spots are generally spaced far apart and sometimes are part of large (tens-of-meters in length) polygonal cracks in the ice. Once

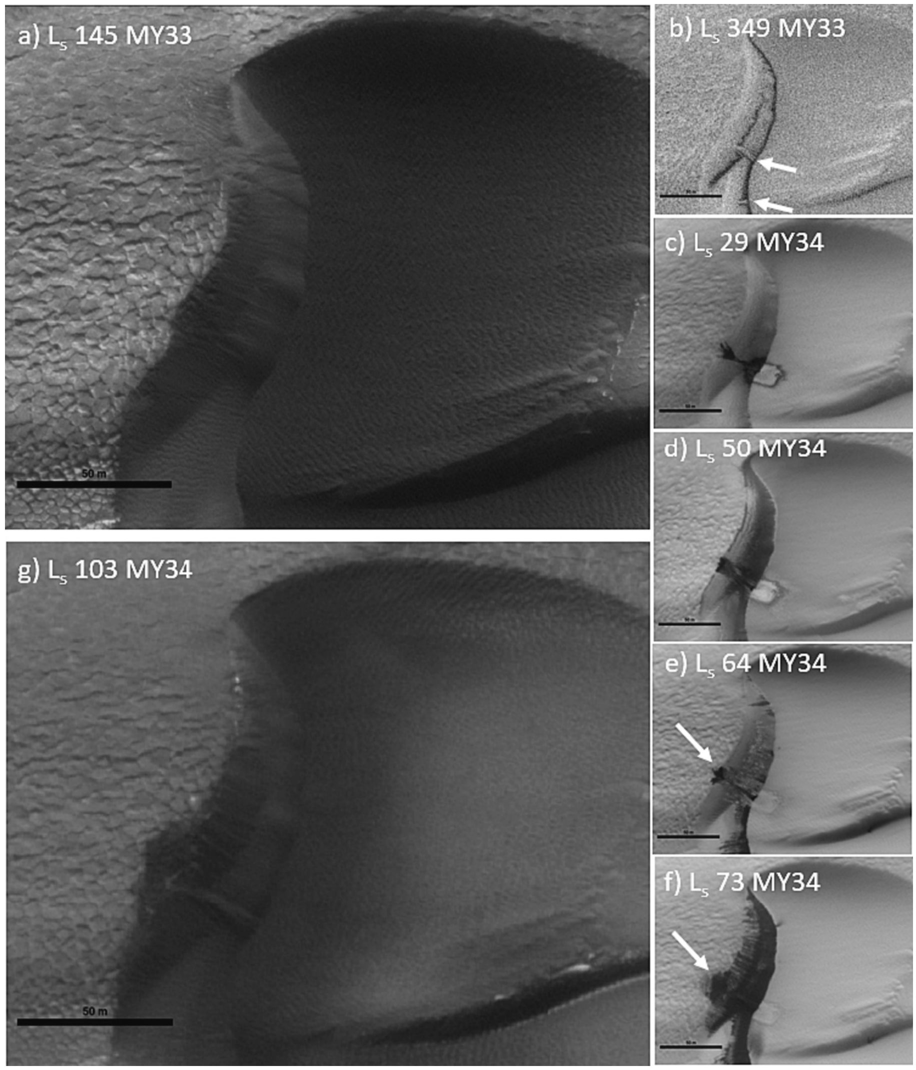

Fig. 10. A dune in Kolhar dune field (84.7 N, 0.7E) that experiences regular frost-induced alcove formation. At least two new alcoves (arrows in b) are visible under the frost (the frost is identified from the uniformly bright surface over the dune and interdune ground, versus the dark, defrosted dune (a, g)). Subsequent springtime sublimation activity (c-f) moved additional sand downslope, extending the dune lee margin due to apron extension of the largest new gully (arrows in e and f). All HiRISE images are illuminated from left and north is up: (a) ESP_045745_2650, (b) ESP_050215_2650, (c) ESP_051283_2650, (d) ESP_051863_2650, (e) ESP_052272_2650, (f) ESP_052562_2650, (g) ESP_053432_2650. Images are not orthorectified, but the bar in each is ~ 50 m.

sublimation is occurring in earnest, sublimation spots densely cover all surfaces (bottom panel of Figs. 8; 12a).

4.4.2. Northern mid-latitude dunes

Consistent high-resolution imaging across the mid-latitude dune fields and the craters that contain them have provided snapshots of varying types of frost coverage and defrosting features that are quite different from polar dunes (Fig. 12b), although some of the same frost-driven activity, such as sandfalls from cracks along the dunes' brink, is observed to occur. Within the northern mid-latitude dunes, the onset of sublimation activity forms spots that are densely packed and that parallel the contours across the stoss slope, suggesting that the seasonal ice layer is weak and easily ruptured. Sublimation spots follow the contours of the dunes.

4.4.3. Southern mid-latitude dunes

In the southern mid-latitudes, early sublimation patterns also occur across a range of slopes, but are not so evidently aligned with the topography (Fig. 12c). Many of the slopes are also dissected with linear gullies and gullies (Section 4.2) and the spots sometimes align with these topographic features, but sometimes not; as described for the northern mid-latitude dunes, this suggests an overall weaker layer of seasonal ice where ruptures are ~equally likely everywhere, not just at points where topography, insolation, or substrate changes would cause a weakness.

4.4.4. Southern high-latitude dunes

Southern high-latitude dunes are often covered with defrosting spots (Fig. 12d) but not always fans (sometimes referred to as "fried eggs"). The evolution of seasonal spots has been comprehensively described in Cesar et al. (2022). Particle size certainly plays a role (Thomas et al., 2011). The wind fields in southern craters may be involved but more study is needed.

5. Summary and discussion

Northern and southern differences in Mars' present-day seasonal activity are driven primarily by the eccentricity of its orbit and the longitude of perihelion. The dramatic difference in elevation of the two hemispheres also plays a role with its effect on the atmospheric pressure and frost point. The southern hemisphere has a significant regional subdivision that occurs as a result of the divergent topography described by Colaprete et al. (2005) that affects how much of the CO_2 ice is derived

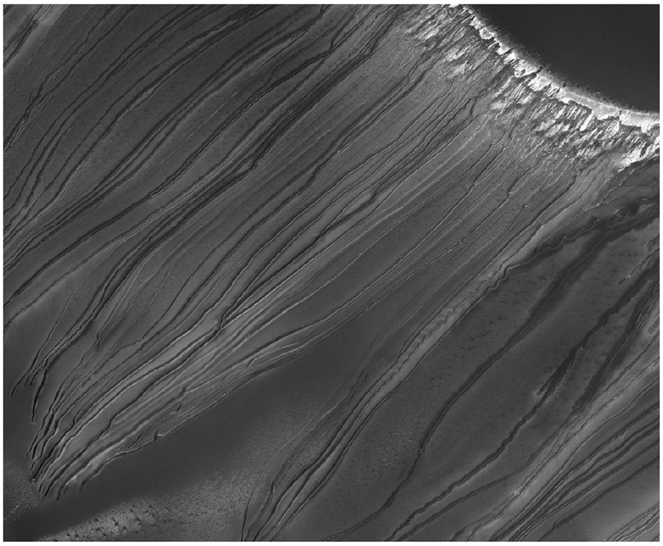

Fig. 11. Linear gullies have formed in some regions of the Russell crater dunes. Note the swaths of ice remaining in the alcoves in the upper right corner of the image. Chunks of ice can be seen in the channels. Image ESP_047078_1255 was taken at 54.26S / 12.95E at L_s 202.2.

from snowfall vs direct deposition.

The long cold southern fall and winter allows more time for CO_2 ice to accumulate and densify in the southern hemisphere. The ice is denser, with a higher "quality" as described in Section 4.2.1. Seasonal ice reaches farther equatorward. More active gully flows are observed in the southern hemisphere, and they are found further equatorward. This could reflect variations in gully activity related to the season of perihelion, with the lowest-latitude northern gullies currently having little or no CO_2 ice formation and thus no activity; if so, the more active hemisphere would reverse over the timescale of perihelion cycles.

In the northern hemisphere we see more snowfall. Northern winter coincides with the perihelion dust storm season, thus the north polar seasonal ice deposits are expected to contain a greater concentration of dust in relation to CO_2 and H_2O ices, as airborne dust provides nuclei for snow to form (Hayne et al., 2014). In the south, in Richardson crater, Andrieu et al., 2018 estimated 0.1% volume of water impurity, which make ~0.17% in mass. In the north Appere et al., 2011, found 0.19% in mass. With less time for densification and more contaminants the seasonal layer of CO_2 ice is likely weaker. At the north polar erg the ice is strong enough to support the Kieffer model of sublimation.

The nature of the surface material enters into the picture when erosion is considered. Araneiform erosion of the SPLD happens in part because the surface is friable but firm enough that channels remain for tens of thousands of years (Piqueux et al., 2003). The surface between sand dunes in the southern hemisphere is eroded into dendritic channels on short (< Mars decade) timescales, perhaps aided by sand abrasion (Portyankina et al., 2017). Conversely, in the north polar region, erosion of the less sandy surface between dunes does not take place. The sand that forms dunes is loose, thus furrows on dunes are easy to erode but quickly erased. Gullies likely reflect a different additional process beyond the Kieffer model, capable of mobilizing boulders on steep slopes. Table 3 summarizes north-south differences.

It is intriguing to consider the role that CO_2 frost processes may have played over Mars's long history. The current frost-formed landforms appear young: araneiforms may have formed within 10^4 years (Piqueux et al., 2003), while formation of well-developed pristine gullies may occur over 10^6–10^7 years (Dundas et al., 2015, 2022). However, CO_2 frost condensation should have been a feature of the Martian climate system throughout its history, as it is predicted by climate models for much higher pressures that occurred in the Noachian and Hesperian periods (Forget et al., 2013). Why do we not observe evidence for much larger frost-eroded landforms? One possibility is that they compete with other processes, such as water ice deposition. Another is that the large gully alcoves in crater walls may already be completely frost-eroded to a stable state. As described in Section 6, these interactions and their variations over time have not been assessed in detail; to do so will require a better understanding of the controls and variability of frost processes and is the logical next step in evaluation of the long-term seasonal processes.

6. Future measurements: working towards a longer climate history

MRO has been carrying out a coordinated campaign of CTX, HiRISE, CRISM, and MCS observations of defrosting variations to understand spatial and temporal differences in frost processes, their physical drivers, volatile flux, and energy balance. After almost a Mars decade of observing with MRO, we have a basic understanding of the relevant physical processes active today, even though they are so different from our own planet. There are still many seasonal activity questions to be addressed, for example the effect of regional and global dust storms on the onset and level of seasonal activity in the south polar region (Hansen et al., 2023). Fully addressing these questions generally will involve a mix of orbital and in situ measurements, as the natural processes of interest occur through a wide range of spatial and temporal scales, e.g., from grain lofting over minutes up to global transport and cycles through seasons as well as solar cycles (Shirley, 2015)).

There is substantial relevant orbital data that has been collected by spacecraft like MRO, and further analysis of those large datasets will yield more insights into connections between observables, like landform morphology and activity timing, with driving environmental conditions and active processes. For example, the Planet Four citizen science project was set up to compare the connection of spring winds to regional circulation models in the south polar region via fan properties (Aye et al., 2019), and a similar project would be worthwhile in the north polar region. The full set of high resolution images of southern araneiforms has not yet been scrutinized to look for small changes, such as those found in the active dendritic troughs (Portyankina et al., 2017), and the extending temporal baseline as well as increased spatial coverage increase the chances of identifying present-day activity.

However, orbital data will need to be acquired through future missions. In particular, high resolution observations at different times of day are needed to capture activity that is happening outside of the narrow time-windows viewable by MRO (Becerra et al., 2021). For example, despite careful monitoring, an image of a jet erupting through the seasonal CO_2 slab ice has not yet been captured, potentially because activity may be concentrated to the morning and midday hours.

Furthermore, new in situ measurements that enable detailed and high-fidelity characterization of surface and atmosphere processes, as they are happening, are needed to test and refine models of those processes appropriate for Mars present-day conditions (summarized in ICE-SAG, 2019; Diniega et al., 2021). Many of the processes of interest are currently explained with terrestrial-based models, from small-scale laboratory studies and/or from analogous terrestrial field studies. Concurrent in situ measurement of wind- or frost-driven activity and the local/regional environment would fill key knowledge gaps that increase the level/number of risks considered in spacecraft, entry-descent-and-landing, and operational designs (i.e., Goal *IV* in MEPAG, 2020) as well as uncertainty in predictions about the active processes and interpretation of geologic and climatic records or habitable environments (i.e., Goals I-III in MEPAG, 2020; Decadal Survey).

An important science challenge is to relate current processes to processes active through different climates. Doing so would enable significantly higher confidence in extrapolating the effects of modern processes from validated models of present-day activity. For example, to understand the climate history of the layers in the north and south polar

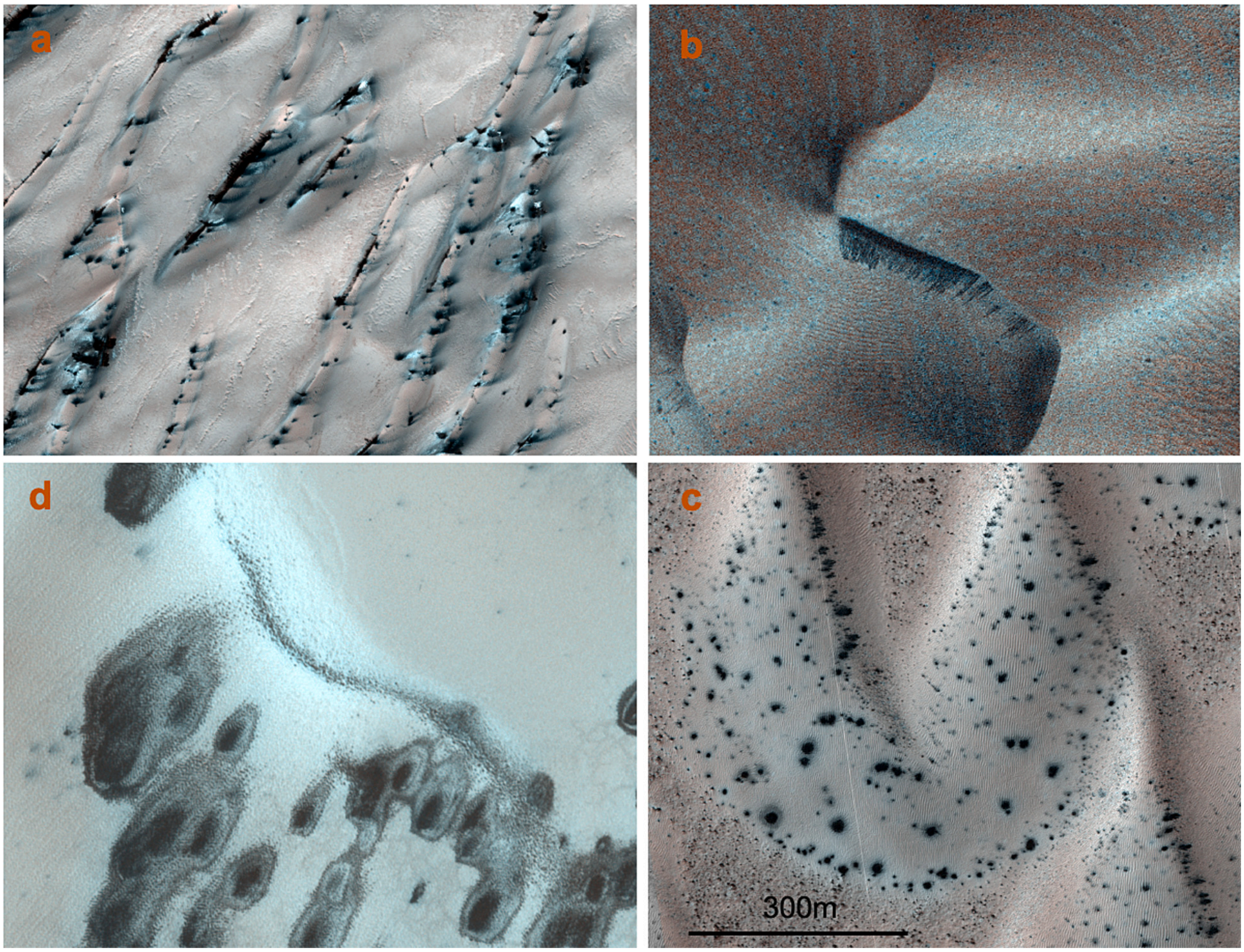

Fig. 12. The character of sublimation activity is distinctly different at northern, mid-, and southern latitudes, despite similar underlying material, which we hypothesize reflects different seasonal ice states in these regions. Images in this figure are from times of year that have roughly the same predicted mean thickness of seasonal ice, ~10 cm, and are representative of the appearance of seasonal activity after sublimation has started within each region. The top left image (a), a north polar cutout, from ESP_016952_2630, shows dunes at 82.7°N / 195.6°E, at $L_s = 62°$. The CO_2 ice is cracked along the brink and particles spray out and land in fan-shaped deposits. In the top right image (b), a north mid-latitude cutout from ESP_067529_2385, taken at 58°N / 58.9°E, at $L_s = 335°$, much of the seasonal activity follows the contours of the dunes. The lower right image (c), a south mid-latitude cutout from ESP_020151_1205, taken at 58.97°S / 16.79°E, at $L_s = 180.5°$, is different from the northern mid-latitude image above as spots show less orientation. The lower left image (d), a south polar cutout from ESP_056450_1025, taken at 77.2°S / 115.8°E, at $L_s = 228.8°$, shows sublimation spots, also different from the north polar image above where activity is well-described by the Kieffer model.

Table 3
Summary of seasonal differences.

Property	North	South
Mean Elevation at top of PLD	−2500 m	+4750 m
Approx. CO_2 frostpoint temperature	150 K	143 K
Maximum decrease in atmospheric pressure from Fig. 4	14%	22%
Peak mass of seasonal cap	~3 × 10^{15} kg	~6 × 10^{15} kg
Extent of contiguous seasonal cap	~50° N	~48° S
Contamination of seasonal ice by water, dust	More	Less
Peak ice thickness	Lower	Higher
Strength of ice	Less time to for densification, weaker	Denser, less porous, stronger

layered deposits, an estimate of how much dust and ice is being accumulated or lost from each pole seasonally is needed. The number of years it takes to turn annual micron-thick differences into the resolved layers we see in the SPLD and NPLD directly influences interpretation of multi-annual and longer-term climate shifts from HiRISE images and SHARAD profiles of the PLDs. To address this type of question, future MRO observations are planned to study surface defrosting and atmospheric conditions as a function of latitude, which may serve as a proxy for frost conditions occurring within a single site under varying orbital conditions.

MRO has shown us that Mars is an active, changing place in today's climate - we do not need to look back billions of years to find interesting processes. They exist today, and have likely had profound impacts on martian geology and climate throughout the planet's history. The seasonal behavior of CO_2 is the dominant agent sculpting Mars' landscape today, and variations in how that is occurring around Mars provide key information about the details of those processes as they act now and through Mars's past.

Declaration of Competing Interest

None.

Data availability

The HiRISE image data supporting this study are openly available from the NASA Planetary Data System (PDS) and the HiRISE instrument website (https://www.uahirise.org).

Acknowledgments

We thank the MRO operations team for collecting a great dataset.

Any use of trade, firm, or product names is for descriptive purposes only and does not imply endorsement by the U.S. Government. SD and SP's contribution to this research was carried out at the Jet Propulsion Laboratory, California Institute of Technology, under a contract with the National Aeronautics and Space Administration (80NM0018D0004). The contributions of C.J.H, S.B, A.M, were supported by the Mars Reconnaissance Orbiter High Resolution Imaging Science Experiment.

References

Acharya, P.J., Smith, I.B., Calvin, W.M., 2023. Tracking the northern seasonal cap retreat of mars using computer vision. Icarus 390. https://doi.org/10.1016/j.icarus.2022.115295.

Aharonson, O., Zuber, M.T., Smith, D.E., Neumann, G.A., Feldman, W.C., Prettyman, T. H., 2004. Depth, distribution and density of CO_2 deposition on Mars. JGR 109, E05004.

Aharonson, O., Mackwell, S., Stansbery, E. (Eds.), 2004a. Sublimation at the Base of a Seasonal CO_2 Slab on Mars Lunar and Planetary Institute Conference Abstracts, p. 1918.

Allison, M., McEwen, M., 2000. A post-pathfinder evaluation of areocentric solar coordinates with improved timing recipes for Mars seasonal/diurnal cycles. Planet. Space Sci. 48, 215–235. https://doi.org/10.1016/S0032-0633(99)00092-6.

Alsaeed, N., Hayne, P.O., 2022. Transport of liquid water into the polar regions of Mars through scavenging by CO2 snowfall. JGRE 127 e2022JE007386.

Alsaeed, N.R., Hayne, P.O., Concepcion, V., 2022, June. Seasonal and interannual variability in CO2 snowfall within the martian north polar vortex. In: Seventh International Workshop on the Mars Atmosphere: Modelling and Observations, p. 3303.

Alwarda, R., Smith, I.B., 2021. Stratigraphy and volumes of the units within the massive carbon dioxide ice deposits of Mars. JGRE 126, e06767.

Andrieu, F., Schmidt, F., Douté, S., Chassefière, E., 2018. Ice state evolution during spring in Richardson crater, Mars. Icarus 315, 158–173. https://doi.org/10.1016/j.icarus.2018.06.019. Elsevier BV.

Appere, T., Schmitt, B., Langevin, Y., Doute, S., Pommerol, A., Forget, F., Spiga, A., Gondet, B., Bibring, J.-P., 2011. Winter and spring evolution of northern seasonal deposits on Mars from OMEGA on Mars express. JGR 116, E05001.

Aye, K.-M., et al., 2019. Planet four: probing seasonal winds on Mars by mapping the southern polar CO_2 jet deposits. Icarus 319, 558–598.

Banks, M.E., Byrne, S., Galla, K., McEwen, A.S., Bray, V.J., Dundas, C.M., Fishbaugh, K. E., Herkenhoff, K., Murray, B.C., 2010. Crater population and resurfacing of the martian north polar layered deposits. JGR 115, E08006.

Banks, M.E., Fenton, L.K., Bridges, N.T., Geissler, P.E., Chojnacki, M., Runyon, K.D., Silvestro, S., Zimbelman, J.R., 2018. Patterns in mobility and modification of middle- and high-latitude southern hemisphere dunes on Mars. JGR Planets 123. https://doi.org/10.1029/2018JE005747.

Bapst, J., Bandfield, J.L., Wood, S.E., 2015. Hemispheric asymmetry in martian seasonal surface water ice from MGS TES. Icarus 260, 396–408.

Becerra, P., et al., 2019. Timescales of the climate record in the south polar ice cap of Mars. Geophys. Res. Lett. 46, 7268–7277.

Becerra, P., et al., 2021. Past, present and future of Mars polar science: outcomes and outlook from the 7th international conference on Mars polar science and exploration. PSJ 2, 209. https://doi.org/10.3847/PSJ/ac19a5.

Bibring, J.-P., et al., 2004. Perennial water ice identified in the south polar cap of Mars. Nature 428, 627–630.

Bourke, M.C., Cranford, A., 2011. Seasonal formation of furrows on polar dunes. In: Fifth International Conference on Mars Polar Science, p. 6059.

Brown, A.J., Calvin, W.M., McGuire, P.C., Murchie, S.L., 2010. Compact reconnaissance imaging spectrometer for Mars (CRISM) south polar mapping: first Mars year of observations. J. Geophys. Res. Planets 115. https://doi.org/10.1029/2009je003333.

Brown, A.J., Calvin, W.M., Murchie, S.L., 2012. Compact reconnaissance imaging spectrometer for Mars (CRISM) north polar springtime recession mapping: first 3 Mars years of observations. J. Geophys. Res. Planets 117. https://doi.org/10.1029/2012je004113.

Buhler, P.B., Piqueux, S., 2021. Obliquity driven CO_2 exchange between Mars' atmosphere, regolith, and polar cap. JGR Planets 126, e06759.

Byrne, S., Ingersoll, A.P., 2003. A sublimation model for martian south polar ice features. Science. https://doi.org/10.1126/science.1080497.

Byrne, S., Zuber, M.T., Neumann, G.A., 2008. Interannual and seasonal behavior of martian residual ice-cap albedo. Planet. Space Sci. 56, 194–211.

Calvin, W.M., Martin, T.Z., 1994. Spatial variability in the seasonal south polar-cap of Mars. J. Geophys. Res. Planets 99 (E10), 21143–21152.

Calvin, W.M., Roach, L.H., Seelos, F.P., Seelos, K.D., Green, R.O., Murchie, S.L., Mustard, J.F., 2009. Compact reconnaissance imaging spectrometer for Mars observations of northern martian latitudes in summer. J. Geophys. Res. Planets 114. https://doi.org/10.1029/2009je003348.

Calvin, W.M., James, P.B., Cantor, B.A., Dixon, E.M., 2015. Interannual and seasonal changes in the north polar ice deposits of Mars: observations from MY 29-31 using MARCI. Icarus 251, 181–190. https://doi.org/10.1016/j.icarus.2014.08.026.

Calvin, W.M., Cantor, B.A., James, P.B., 2017. Interannual and seasonal changes in the south seasonal polar cap of Mars: observations from MY 28-31 using MARCI. Icarus 292, 144–153. https://doi.org/10.1016/j.icarus.2017.01.010.

Cartwright, S.F.A., Calvin, W.M., Seelos, K.D., Seelos, F.P., 2022. Characterizing Seasonal and Residual Ices at the South Pole of Mars using a Universal Set of CRISM Spectral Endmembers. https://doi.org/10.1029/2022JE007372.

Cesar, C., Pommerol, A., Thomas, N., Portyankina, G., Hansen, C.J., Tornabene, L., Munaretto, G., Cremonese, G., 2022. Seasonal southern circum-polar spots and araneiforms observed with the color and stereo surface imaging system (CaSSIS). PSS 224, 105593.

Colaprete, A., Toon, O.B., 2002. Carbon dioxide snow storms during the polar night on Mars. JGR Planets 107. https://doi.org/10.1029/2001JE001758.

Colaprete, A., Haberle, R.M., Toon, O.B., 2003. Formation of convective carbon dioxide clouds near the south pole of Mars. JGR Planets 108. https://doi.org/10.1029/2003JE02053.

Colaprete, A., Barnes, J., Haberle, R.M., Hollingsworth, J.L., Kieffer, H.H., Titus, T.N., 2005. Albedo of the south pole on Mars determined by topographic forcing of atmosphere dynamics. Nature 435, 184–188.

Conway, S.J., de Haas, T., Harrison, T.N., 2019. Martian gullies: a comprehensive review of observations, mechanisms, and insights from earth analogues. Geol. Soc. Lond. Spec. Publ. 467, 7–66. https://doi.org/10.1144/SP467.14.

Cornwall, C., Titus, T.N., 2009. Spatial and temporal distributions of martian north polar cold spots before, during, and after the global dust storm of 2001. J. Geophys. Res. Planets 114 (E2).

Cornwall, C., Titus, T.N., 2010. A comparison of martian north and south polar cold spots and the long-term effects of the 2001 global dust storm. J. Geophys. Res. Planets 115 (E6).

Cushing, G.E., Titus, T.N., 2008. MGS-TES thermal inertia study of the Arsia Mons caldera. JGR 113, E06006.

De Haas, T., McArdell, B.W., Conway, S.J., McElwaine, J.N., Kleinhans, M.G., Salese, F., Grindrod, P.M., 2019. Initiation and flow conditions of contemporary flows in martian gullies. J. Geophys Res. Planets 124, 2,246–2,271. https://doi.org/10.1029/2018JE005899.

Diniega, S., Byrne, S., Bridges, N.T., Dundas, C.M., McEwen, A.S., 2010. Seasonality of present-day martian dune-gully activity. Geology 38, 1,047–1,050. https://doi.org/10.1130/G31287.1.

Diniega, S., Hansen, C.J., Hugenholtz, C., Dundas, C., 2013. A new dry hypothesis for the formation of martian linear gullies. Icarus 225, 526–537.

Diniega, S., et al., 2021. Modern Mars' geomorphological activity, driven by wind, frost, and gravity. Geomorphology 2021 (380), 107627.

Dinwiddie, C., Titus, T., 2021. Airborne dust plumes lofted by dislodged ice blocks at Russell Crater, Mars. GRL 48 e2020GL091920.

Doute, S., Schmitt, B., Langevin, Y., Bibring, J.P., Altieri, F., Bellucci, G., Gondet, B., Poulet, F., 2007. South pole of Mars: nature and composition of the icy terrains from Mars express OMEGA observations. Planet. Space Sci. 55 (1–2), 113–133.

Dundas, C.M., Diniega, S., Hansen, C.J., Byrne, S., McEwen, A.S., 2012. Seasonal activity and morphological changes in martian gullies. Icarus 220, 124–143.

Dundas, C.M., Diniega, S., McEwen, A.S., 2015. Long-term monitoring of martian gully formation and evolution with MRO/HiRISE. Icarus 251, 244–263. https://doi.org/10.1016/j.icarus.2014.05.013.

Dundas, C.M., McEwen, A.S., Diniega, S., Hansen, C.J., Byrne, S., McElwaine, J.N., 2019. The formation of gullies on Mars today. Geol. Soc. Lond. Spec. Publ. 467, 67–94. https://doi.org/10.1144/SP467.5.

Dundas, C.M., Conway, S.J., Cushing, G.E., 2022. Martian gully activity and the gully sediment transport system. Icarus 386, 115133. https://doi.org/10.1016/j.icarus.2022.115133.

Edgett, K.S., Christensen, P.R., 1991. The particle size of martian aeolian dunes. JGR Planets 96, 22765–22776.

Eluszkiewicz, J., Moncet, J.-L., 2003. A coupled microphysical / radiative transfer model of albedo and emissivity of planetary surfaces covered by volatile ices. Icarus 166, 375–384.

Eluszkiewicz, J., Moncet, J.-L., Titus, T.N., Hansen, G.B., 2005. A microphysically-based approach to modeling emissivity and albedo of the martian seasonal caps. Icarus 174, 524–534.

Fenton, L.K., Hayward, R.K., 2010. Southern high latitude dune fields on Mars: morphology, aeolian inactivity, and climate change. Geomorphology 121, 98–121.

Forget, F., Hansen, G.B., Pollack, J.B., 1995. Low brightness temperatures of martian polar caps: CO_2 clouds or low surface emissivity? JGR 100, 21219–21234.

Forget, F., Hourdin, F., Talagrand, O., 1998. CO2 snowfall on Mars: simulation with a general circulation model. Icarus 131, 302–316.

Forget, F., Wordsworth, R., Millour, E., Madeleine, J.-B., Kerber, L., Leconte, J., Marcq, E., Haberle, R.M., 2013. 3D modelling of the early martian climate under a denser CO2 atmosphere: temperatures and CO_2 ice clouds. Icarus 222, 81–99.

Gary-Bicas, C.E., Hayne, P.O., Horvath, T., Heavens, N.G., Kass, D.M., Kleinboehl, A., et al., 2020. Asymmetries in snowfall, emissivity, and albedo of Mars' seasonal polar caps: Mars climate sounder observations. J. Geophys. Res. Planets 125. https://doi.org/10.1029/2019JE006150 e2019JE006150.

Hansen, C.J., Thomas, N., Portyankina, G., McEwen, A., Becker, T., Byrne, S., Herkenhoff, K., Kieffer, H., Mellon, M., 2010. HiRISE observations of gas sublimation-driven activity in Mars' southern polar regions: I. Erosion of the surface. Icarus 205, 283–295.

Hansen, C.J., Bourke, M., Bridges, N.T., Byrne, S., Colon, C., Diniega, S., Dundas, C., Herkenhoff, K., McEwen, A., Mellon, M., Portyankina, G., Thomas, N., 2011.

Seasonal erosion and restoration of Mars' northern polar dunes. Science 331, 575–578.
Hansen, C.J., Byrne, S., Portyankina, G., Bourke, M., Dundas, C., McEwen, A., Mellon, M., Pommerol, A., Thomas, N., 2013. Observations of the northern seasonal polar cap on Mars: I. Spring sublimation activity and processes. Icarus 225, 881–897.
Hansen, C.J., Diniega, S., Hayne, P.O., 2018. Mars' snowfall and sand avalanches. LPSC 49, 2175. LPI Contribution No. 2083.
Hansen, C.J., Aye, K.-M., Portyankina, G., Schwamb, M., Michaels, T., Tamppari, L., 2023. A nine year record of interannual variability of seasonal activity in Mars' south polar region dubbed "Manhattan". LPSC 2023, 2315.
Hao, J., Michael, G.G., Adeli, S., Jaumann, R., Portyankina, G., Hauber, E., Millot, C., Zuschneid, W., 2020. Variability of spider spatial configuration at the martian south pole. P&SS 185. https://doi.org/10.1016/j.pss.2020.104848.
Harrison, T.N., Gordon, G.R., Tornabene, L.L., Jones, E., 2015. Global documentation of gullies with the Mars Reconnaissance Orbiter context camera and implications for their formation. Icarus 252, 236–254.
Hayne, P.O., Paige, D.A., Schofield, J.T., Kass, D.M., Kleinbohl, A., Heavens, N.G., McCleese, D.J., 2012. Carbon dioxide snow clouds on Mars: south polar winter observations by the Mars climate sounder. JGR 117. https://doi.org/10.1029/2011JE004040.
Hayne, P., Paige, D.A., Heavens, N.G., 2014. The role of snowfall in forming the seasonal ice caps of Mars: models and constraints from Mars climate sounder. Icarus 231, 122–130.
Hayward, R.K., 2011. Mars global digital dune database (MGD^3): north polar region (MC-1) distribution, applications, and volume estimates. Earth Surf. Process. Landf. https://doi.org/10.1002/esp.2219.
Hayward, R.K., Fenton, L.K., Tanaka, K.L., Titus, T.N., Colaprete, A., Christensen, P.R., 2010. Mars Global Digital Dune Database; MC-1. U.S. Geological Survey Open-File Report 2010–1170. https://doi.org/10.3133/ofr20101170.
Hayward, R.K., Fenton, L.K., Titus, T.N., 2014. Mars global digital dune database (MCD3): global dune distribution and wind pattern observations. Icarus 230, 38–46. https://doi.org/10.1016/j.icarus.2013.04.011.
Herkenhoff, K.E., Plaut, J.J., 2000. Surface ages and resurfacing rates of the polar layered deposits on Mars. Icarus 144 (2), 243–253. https://doi.org/10.1006/icar.1999.6287.
Herschel, W., 1784. On the remarkable appearances at the polar regions of the plaen Mars, the inclination of its axis, the position of its poles, and its spheroidical figure; with a few hints relating to its real diameter and atmosphere. Philos. Trans. R. Soc. Lond. 74 (233–73), 1784.
Hoffman, N., 2002. Active polar gullies on Mars and the role of carbon dioxide. Astrobiology 2, 313–323. https://doi.org/10.1089/153110702762027899.
Hvidberg, C.S., Fishbaugh, K.E., Winstrup, M., Svensson, A., Byrne, S., Herkenhoff, K.E., 2012. Reading the climate record of the martian polar layered deposits. Icarus 221, 405–419.
James, P.B., Kieffer, H.H., Paige, D.A., 1992. The seasonal cycle of carbon dioxide on Mars. In: Kieffer, H.H., et al. (Eds.), Mars. University of Arizona Press, Tucson, pp. 934–969.
Kass, D.M., et al., 2020. Mars Climate Sounder Observation of Mars' 2018 Global Dust Storm. Geophys. Res. Lett. 47 (23), e83931.
Kelly, N.J., Boynton, W.V., Kerry, K., Hamara, D., Janes, D., Reedy, R.C., Kim, K.J., Haberle, R.M., 2006. Seasonal polar carbon dioxide frost on Mars: CO_2 mass and columnar thickness distribution. JGR 111, E03S07. https://doi.org/10.1029/2006JE002678.
Kieffer, H., 2007. Cold jets in the martian polar cap. JGR 112, E08005.
Kieffer, H.H., Titus, T.N., 2001. TES mapping of Mars' north seasonal cap. Icarus 154 (1), 162–180.
Kieffer, H., Titus, T., Mullins, K., Christensen, P., 2000. Mars south polar spring and summer behavior observed by TES: seasonal cap evolution controlled by grain size. JGR 105, 9653–9700.
Kieffer, H.H., Christensen, P.R., Titus, T.N., 2006. CO2 jets formed by sublimation beneath translucent slab ice in Mars' seasonal south polar ice cap. Nature 442 (7104), 793–796.
Koutnik, M., Byrne, S., Murray, B., 2002. South Polar Layered Deposits of Mars: The cratering record. J. Geophys. Res. Planets 107, 5100-10–10 (2002).
Landis, M.E., et al., 2023. Polar science results from Mars Reconnaissance Orbiter: multiwavelength, multiyear insights. Icarus (2023). doi: 10.1016/j. icarus2023115794.
Landis, M.E., Byrne, S., Daubar, I.J., Herkenhoff, K.E., Dundas, C.M., 2016. A revised surface age for the north polar layered deposits of Mars. Geophys. Res. Lett. 43 (7), 3060–3068. https://doi.org/10.1002/2016GL068434.
Lange, L., Forget, F., Banfield, D., Wolff, M., Spiga, A., Millour, E., Viúdez-Moreiras, D., Bierjon, A., Piqueux, S., Newman, C., Pla-García, J., Banerdt, W.B., 2022. Insight pressure data recalibration, and its application to the study of long-term pressure changes on Mars. J. Geophys. Res. Planets 127 (5). https://doi.org/10.1029/2022JE007190.
Langevin, Y., Doute, S., Vincendon, M., Poulet, F., Bibring, J.P., Gondet, B., Schmitt, B., Forget, F., 2006. No signature of clear CO2 ice from the 'cryptic' regions in Mars' south seasonal polar cap. Nature 442 (7104), 790–792.
Langevin, Y., Bibring, J.P., Montmessin, F., Forget, F., Vincendon, M., Doute, S., Poulet, F., Gondet, B., 2007a. Observations of the south seasonal cap of Mars during recession in 2004-2006 by the OMEGA visible/near-infrared imaging spectrometer on board Mars express. J. Geophys. Res. Planets 112 (E8). https://doi.org/10.1029/2006je002841.
Langevin, Y., Bibring, J.-P., Montmessin, F., Forget, F., Vincendon, M., Douté, S., Poulet, F., Gondet, B., 2007b. Observations of the south seasonal cap of Mars during recession in 2004–2006 by the OMEGA visible/near-infrared imaging spectrometer on board Mars express. J. Geophys. Res. Planets 112, 8. https://doi.org/10.1029/2006JE002841.
Laskar, J., Levrard, B., Mustard, J.F., 2002. Orbital forcing of the martian polar layered deposits. Nature 419, 375–377.
Laskar, J., Correia, A.C.M., Gastineau, M., Joutel, F., Levrard, B., Robutel, P., 2004. Long-term evolution and chaotic diffusion of the insolation quantities of Mars. Icarus 170, 343–364.
Leighton, R.B., Murray, B.C., 1966. Behavior of carbon dioxide and other volatiles on Mars. Science 153, 136–144.
Levrard, B., Forget, F., Montmessin, F., Laskar, J., 2007. Recent formation and evolution of northern martian polar layered deposits as inferred from a global climate model. JGR 112. https://doi.org/10.1029/2006JE002772.
Malin, M.C., Edgett, K.S., 2001. Mars global surveyor Mars orbiter camera: interplanetary cruise through primary mission. JGR 106, 23429–23570.
Malin, M.C., et al., 2001. The Mars color imager (MARCI) on the Mars climate orbiter. J. Geophys. Res. 106, 17651–17672.
Malin, M.C., et al., 2007. Context camera investigation on board the Mars Reconnaissance Orbiter. J. Geophys. Res. 112, E05S04.
Matsuo, K., Heki, K., 2009. Seasonal and interannual changes of volume density of martian CO2 snow from time-variable elevation and gravity. Icarus 202, 90–94.
Mc Keown, L.E., Bourke, M.C., McElwaine, J., 2017. Experiments on sublimating carbon dioxide ice and implications for contemporary surface processes on Mars. Sci. Rep. 7, 14181.
Mc Keown, L.E., McElwaine, J.N., Bourke, M.C., Sylvest, M.E., Patel, M.R., 2021. The formation of araneiforms by carbon dioxide venting and vigorous sublimation dynamics under martian atmospheric pressure. Sci. Rep. 11, 6445.
Mc Keown, L.E., Diniega, S., Portyankina, G., Hansen, C.J., Aye, K.-M., Piqueux, S., Scully, J.E.C., 2023. Martian araneiforms: a review. JGR Planets 128. https://doi.org/10.1029/JE007684.
McCleese, D.J., et al., 2007. Mars climate sounder: an investigation of thermal and water vapor structure, dust and condensate distributions in the atmosphere, and energy balance of the polar regions. J. Geophys. Res. 112 (E5), E05S06.
McCleese, D.J., et al., 2008. Intense polar temperature inversion in the middle atmosphere on Mars. Nat. Geosci. 1, 745–749.
McEwen, A.S., et al., 2007. Mars Reconnaissance Orbiter's high resolution imaging science experiment (HiRISE). J. Geophys. Res. 112, E05S02.
McEwen, A.S., et al., 2023. The High-Resolution Imaging Science Experiment (HiRISE) in the MRO Extended Science Phases (2009–2022). Icarus (2023). doi:10.1016/j. icarus.2023.115795.
Mischna, M.A., Richardson, M., Wilson, R., McCleese, D.J., 2003. On the orbital forcing of Martian water and CO_2 cycles: a general circulation model study with simplified volatile schemes. JGR Planets 108. https://doi.org/10.1029/2003JE002051.
Mount, C.P., Titus, T.N., 2015. Evolution of Mars' nothern polar seasonal CO2 deposits: variations in surface brightness and bulk density. JGR Planets 120, 1252–1266.
Murchie, S.L., et al., 2007. Compact Reconnaissance Imaging Spectrometer for Mars (CRISM) on Mars Reconnaissance Orbiter (MRO). J. Geophys. Res. 112, E05S03. https://doi.org/10.1029/2006JE002682.
Murray, B.C., Ward, W.R., Yeoung, S.C., 1973. Periodic insolation variations on Mars. Science 180, 638–640.
Neugebauer, G., Münch, G., Kieffer, H., Chase Jr., S.C., Miner, E., 1971. Mariner 1969 infrared radiometer results: temperatures and thermal properties of the martian surface. Astron. J. 76, 719. https://doi.org/10.1086/111189.
Ordonez-Etxeberria, I., Hueso, R., Sánchez-Lavega, A., Millour, E., Forget, F., 2019. Meteorological pressure at Gale crater from a comparison of REMS/MSL data and MCD modelling: effect of dust storms. Icarus 317, 591–609. https://doi.org/10.1016/j.icarus.2018.09.003.
Pasquon, K., Gargani, J., Masse, M., Conway, S.J., 2016. Present-day formation and seasonal evolution of linear dune gullies on Mars. Icarus 274, 195–210. https://doi.org/10.1016/j.icarus.2016.03.024. Elsevier BV.
Pasquon, K., Gargani, J., Massé, M., Vincendon, M., Conway, S.J., Séjourné, A., Jomelli, V., Balme, M.R., Lopez, S., Guimpier, A., 2019. Present-day development of gully-channel sinuosity by carbon dioxide gas supported flows on Mars. Icarus 329, 296–313. https://doi.org/10.1016/j.icarus.2019.03.034. Elsevier BV.
Phillips, R.J., et al., 2011. Massive CO2 ice deposits sequestered in the south polar layered deposits of Mars. Science 322, 838.
Pilorget, C., Forget, F., 2015. Formation of gullies on Mars by debris flows triggered by CO_2 sublimation. Nat. Geosci. 9, 65–69. https://doi.org/10.1038/NGEO2619.
Pilorget, C., Forget, F., Millour, E., Vincendon, M., Madeleine, J., 2011. Dark spots and cold jets in the polar regions of Mars: new clues from a thermal model of surface CO2 ice. Icarus 213, 131–149. https://doi.org/10.1016/j.icarus.2011.01.031.
Piqueux, S., Christensen, P.R., 2008. North and south subice gas flow and venting of the seasonal caps of Mars: a major geomorphological agent. JGR 113, E06005.
Piqueux, S., Byrne, S., Richardson, M., 2003. The sublimation of Mars' southern seasonal CO_2 ice cap and the formation of spiders. J. Geophys. Res. 108 (E8), 3-1.
Piqueux, S., Edwards, C.S., Christensen, P.R., 2008. Distribution of the ices exposed near the south pole of Mars using thermal emission imaging system (THEMIS) temperature measurements. J. Geophys. Res. Planets 113 (E8). https://doi.org/10.1029/2007je003055.
Piqueux, S., Kleinbohl, A., Hayne, P.O., Kass, D.M., Schofield, J.T., McCleese, D.J., 2015a. Variability of the martian seasonal CO_2 cap extent over eight Mars years. Icarus 251, 164–180. https://doi.org/10.1016/j.icarus.2014.10.045.
Piqueux, S., Byrne, S., Kieffer, H.H., Titus, T.N., Hansen, C.J., 2015b. Enumeration of Mars years and seasons since the beginning of telescopic exploration. Icarus 251, 332–338.

Piqueux, S., Kleinbohl, A., Hayne, P.O., Heavens, N.G., Kass, D.M., McCleese, D.J., Schofield, J.T., Shirley, J.H., 2016. Discovery of a widespread low-latitude diurnal CO_2 frost cycle on Mars. JGR 121, 1174–1189.

Piqueux, S., Hayne, P.O., Kleinböhl, A., Kass, D.M., Schreier, M., McCleese, D.J., Shirley, J.H., 2023. Atmospheric CO2 depletion near the surface in the martian polar regions. J. Geophys. Res. Planets 128 (6) e2022JE007332.

Pommerol, A., Portyankina, G., Thomas, N., Aye, K.M., Hansen, C.J., Vincendon, M., Langevin, Y., 2011. Evolution of south seasonal cap during martian spring: insights from high-resolution observations by HiRISE and CRISM on Mars Reconnaissance Orbiter. J. Geophys. Res. Planets 116. https://doi.org/10.1029/2010je003790.

Portyankina, G., Markiewicz, W.J., Thomas, N., Hansen, C.J., Milazzo, M., 2010. HiRISE observations of gas sublimation-driven activity in Mars' southern polar regions: III. Models of processes involving translucent ice. Icarus 205, 311–320.

Portyankina, G., Pommerol, A., Aye, K.-M., Hansen, C.J., Thomas, N., 2012. Polygonal cracks in the seasonal semi-translucent CO_2 ice layer in martian polar areas. J. Geophys. Res. https://doi.org/10.1029/2011JE003917.

Portyankina, G., Pommerol, A., Aye, K.-M., Hansen, C.J., Thomas, N., 2013. Observations of the northern seasonal polar cap on Mars II: HiRISE photometric analysis of northern polar dunes in spring. Icarus 225, 898–910.

Portyankina, G., Hansen, C.J., Aye, K.-M., 2017. Present-day erosion of martian polar terrain by the seasonal CO_2 jets. Icarus 282, 93–103.

Portyankina, G., Merrison, J., Iversen, J.J., Youldi, Z., Hansen, C.J., Aye, K.-M., Pommerol, A., Thomas, N., 2019. Laboratory investigations of the physical state of CO2 ice in a simulated martian environment. Icarus 322, 210–220.

Portyankina, G., Aye, K.-M., Schwamb, M.E., Hansen, C.J., Michaels, T.I., Lintott, C.J., 2022. Planet four: derived south polar martian winds interpreted using mesoscale modeling. PSJ 3, 31.

Putzig, N.E., Mellon, M.T., 2007. Apparent thermal inertia and the surface heterogeneity of Mars. Icarus 191, 68–94. https://doi.org/10.1016/j.icarus.2007.05.013.

Schmidt, F., Douté, S., Schmitt, B., Vincendon, M., Bibring, J.-P., Langevin, Y., 2009. Albedo control of seasonal South Polar cap recession on Mars. Icarus 200, 374–394. https://doi.org/10.1016/j.icarus.2008.12.014.

Schmidt, F., Schmitt, B., Doute, S., Forget, F., Jian, J.J., Martin, P., Langevin, Y., Bibring, J.P., Team, O., 2010. Sublimation of the martian CO_2 seasonal south polar cap. Planet. Space Sci. 58 (10), 1129–1138. https://doi.org/10.1016/j.pss.2010.03.018.

Schorghofer, N., Edgett, K.S., 2006. Seasonal surface frost at low latitudes on Mars. Icarus 180, 321–334. https://doi.org/10.1016/j.icarus.2005.08.022.

Schwamb, M.E., Aye, K.-M., Portyankina, G., Hansen, C.J., Campbell, A., Allen, S., Calef III, F.J., Duca, S., McMaster, A., Miller, G.R.M., 2018. Planet four: terrains - discovery of araneiforms outside of the south polar layered deposits. Icarus 308, 148–187. https://doi.org/10.1016/j.icarus.2017.06.017.

Seu, R., et al., 2007. SHARAD sounding radar on the Mars Reconnaissance Orbiter. J. Geophys. Res. 112 https://doi.org/10.1029/2006JE002745.

Shirley, J.H., 2015. Solar system dynamics and global-scale dust storms on Mars. Icarus 251, 128–144.

Smith, D.E., Zuber, M.T., Neumann, G.A., 2001a. Mars orbiter laser altimeter: experiment summary after the first year of global mapping of Mars. J. Geophys. Res. Planets 106 (E10), 23689–23722.

Smith, D.E., Zuber, M.T., Neumann, G.A., 2001b. Seasonal variation of snow depth on Mars. Science 294, 2141–2146.

Smith, I.B., et al., 2020. The holy grail: a road map for unlocking the climate record stored within Mars' polar layered deposits. Planet. Space Sci. 184, 104841.

Tanaka, K.L., Robbins, S.J., Fortezzo, C.M., Skinner, J.A., Hare, T.M., 2014. The digital global geologic map of Mars: chronostratigraphic ages, topographic and crater morphologic characteristics, and updated resurfacing history. Planet. Space Sci. 95, 11–24. https://doi.org/10.1016/j.pss.2013.03.006.

Thomas, N., Hansen, C.J., Portyankina, G., Russell, P., 2010. HiRISE observations of gas sublimation-driven activity in Mars' southern polar regions: II. Surficial deposits and their origins. Icarus 205, 296–310.

Thomas, N., Portyankina, G., Hansen, C.J., Pommerol, A., 2011. Sub-surface CO_2 gas flow in Mars' polar regions: gas transport under constant production rate conditions. GRL 38 (8), L08203.

Thomas, N., et al., 2017. The colour and stereo surface imaging system (CaSSIS) for the ExoMars trace gas orbiter. Space Sci. Rev. 212 (3–4), 1897–1944.

Thomas, P.C., Calvin, W.M., James, P.B., 2020. Debris accumulations of CO2 ice in the south polar residual cap of mars: longevity and processes. Icarus 341, 113625. https://doi.org/10.1016/j.icarus.2020.113625.

Tillman, J., Johnson, N.C., Guttorp, P., Percival, D.B., 1993. The martian annual atmospheric pressure cycle: years without great dust storms. JGR 98, 10963–10971.

Titus, T.N., 2005. Thermal infrared and visual observations of a water ice lag in the Mars southern summer. GRL 32. https://doi.org/10.1029/2005GL024211.

Titus, T.N., Kieffer, H.H., Mullins, K.F., Christensen, P.R., 2001. TES premapping data: slab ice and snow flurries in the martian north polar night. JGR 106, 23181–23196.

Titus, T.N., Kieffer, H.H., Christensen, P.R., 2003. Exposed water ice discovered near the south pole of Mars. Science 299, 1048–1051.

Titus, T.N., Calvin, W.M., Kieffer, H.H., Langevin, Y., Prettyman, T.H., 2008. Martian polar processes. In: Bell, J. (Ed.), The Martian Surface. Cambridge University Press.

Valantinas, A., et al., 2023. Tropical Frost on Martian Volcanoes. LPSC 54 Contribution 2806, Abstract ID 1539.

Vincendon, M., 2015. Identification of Mars gully activity types associated with ice composition. J. Geophys. Res. Planets 120 (1), 859–1,879. https://doi.org/10.1002/2015JE004909.

Vincendon, M., Forget, F., Vincendon, M., Forget, F., Mustard, J., 2010. Water ice at low to midlatitudes on Mars. J. Geophys. Res. 115 (E10), E10001 https://doi.org/10.1029/2010JE003584.

Wagstaff, K.L., Titus, T.N., Ivanov, A.B., Castano, R., Bandfield, J.L., 2008. Observations of the north polar water ice annulus on Mars using THEMIS and TES. P&SS 56, 256–265.

Waugh, D.W., Toigo, A.D., Guzewich, S.D., Greybush, S.J., Wilson, R.J., Montabone, L., 2016. Martian polar vortices: comparison of reanalyses. JGR Planets 121, 1770–1785.

Widmer, J.M., Diniega, S., 2019. Constraining environmental conditions for dune-alcove formation in the northern mid-latitude region of Mars. In: Ninth International Conference on Mars Mars, LPI Contribution No. 2089, p. 6147.

Widmer, J.M., Diniega, S., Hayne, P.O., 2023. A global look at martian CO2 snowfall using observations from the Mars climate sounder. LPSC 54, 2262. LPI Contribution No. 2806.

Xiao, H., Stark, A., Schmidt, F., Hao, J., Steinbrügge, G., Wagner, N.L., Su, S., Cheng, Y., Oberst, J., 2022a. Spatio-temporal level variations of the martian seasonal north polar cap from co-registration of MOLA profiles. J. Geophys. Res. Planets 127. https://doi.org/10.1029/2021JE007158 e2021JE007158.

Xiao, H., Stark, A., Schmidt, F., Hao, J., Su, S., Steinbrügge, G., Oberst, J., 2022b. Spatio-temporal level variations of the martian seasonal south polar cap from co-registration of MOLA profiles. J. Geophys. Res. Planets 127. https://doi.org/10.1029/2022je007196. American Geophysical Union (AGU). e2022JE007196.

Zhao, Y., Zhong, L., Yuan, R., Zhao, C., Li, R., Wang, Y., Richardson, M.I., 2021. Simulation of martian dust effects on polar CO_2 ice caps and atmospheric circulation using the marswrf model. J. Geophys. Res. Planets 126 (12). https://doi.org/10.1029/2021JE006937 e2021JE006937.

Zuber, M., et al., 1998. Observations of the north polar region of Mars from the Mars orbiter laser altimeter. Science 282, 23.

Zurek, R.W., Smrekar, S.E., 2007. An overview of the Mars Reconnaissance Orbiter (MRO) science mission. J. Geophys. Res. Planets 112, 1–22.